Electronic Supplementary Information
for

Are the metal identity and stoichiometry of metal complexes important for colchicine site binding and inhibition of tubulin polymerization?

Iuliana Besleaga,[a] Renáta Raptová,[b,c] Alexandru-Constantin Stoica,[d] Miljan N. M. Milunovic,[a,*] Michal Zalibera,[b] Ruoli Bai,[e] Nóra Igaz,[f] Jóhannes Reynisson,[g] Mónika Kiricsi,[g] Éva A. Enyedy,[h,i,*] Peter Rapta,[b] Ernest Hamel,[e] Vladimir B. Arion[a,d,*]

[a]*Institute of Inorganic Chemistry, University of Vienna, A-1090 Vienna, Austria*
[b]*Institute of Physical Chemistry and Chemical Physics, Faculty of Chemical and Food Technology, Slovak University of Technology in Bratislava, SK-81237 Bratislava, Slovakia*
[c]*Institute of Physical and Theoretical Chemistry, Graz University of Technology, Stremayrgasse 9/II, A-8010 Graz, Austria*
[d]*Inorganic Polymers Department, "Petru Poni" Institute of Macromolecular Chemistry, Aleea Gr. Ghica Voda 41 A, Iasi 700487, Romania*
[e]*Molecular Pharmacology Branch, Developmental Therapeutics Program, Division of Cancer Diagnosis and Treatment, National Cancer Institute, Frederick National Laboratory for Cancer Research, National Institutes of Health, Frederick, Maryland 21702, United States*
[f]*Department of Biochemistry and Molecular Biology, University of Szeged, Közép fasor 52, H-6726 Szeged, Hungary*
[g]*School of Pharmacy and Bioengineering, Keele University, Newcastle-under-Lyme, Staffordshire ST5 5BG, United Kingdom*
[h]*Department of Molecular and Analytical Chemistry, Interdisciplinary Excellence Centre, University of Szeged, Dóm tér 7-8, H-6720 Szeged, Hungary*
[i]*MTA-SZTE Lendület Functional Metal Complexes Research Group, University of Szeged, Dóm tér 7, H-6720 Szeged, Hungary*

Table of Contents

1. NMR Data

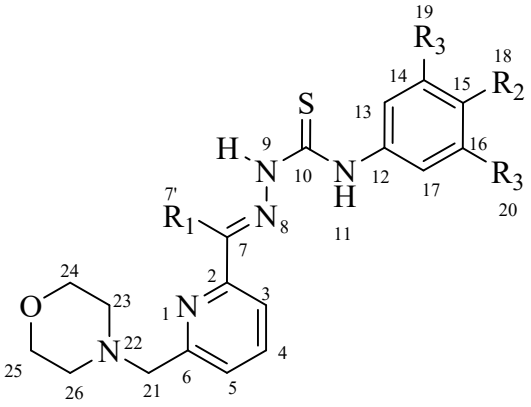

E-isomer

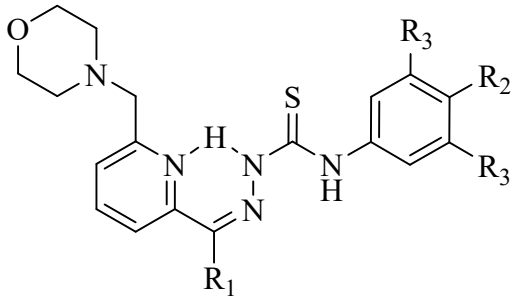

Z-isomer

Chart S1. Atom numbering of ligands for the assignment of NMR resonances.

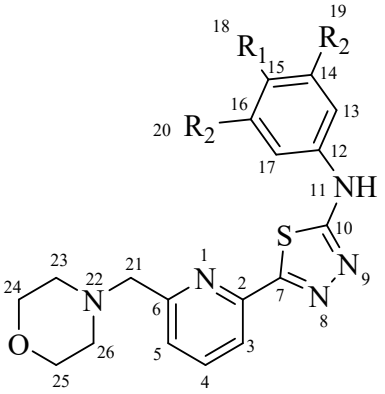

R_1 = OH, R_2 = Me **(H*L*$^{1'}$)**
R_1 = H, R_2 = H **(H*L*$^{3'}$)**

Chart S2. Line drawings of oxidized TSCs and their atom numbering for the assignment of NMR resonances.

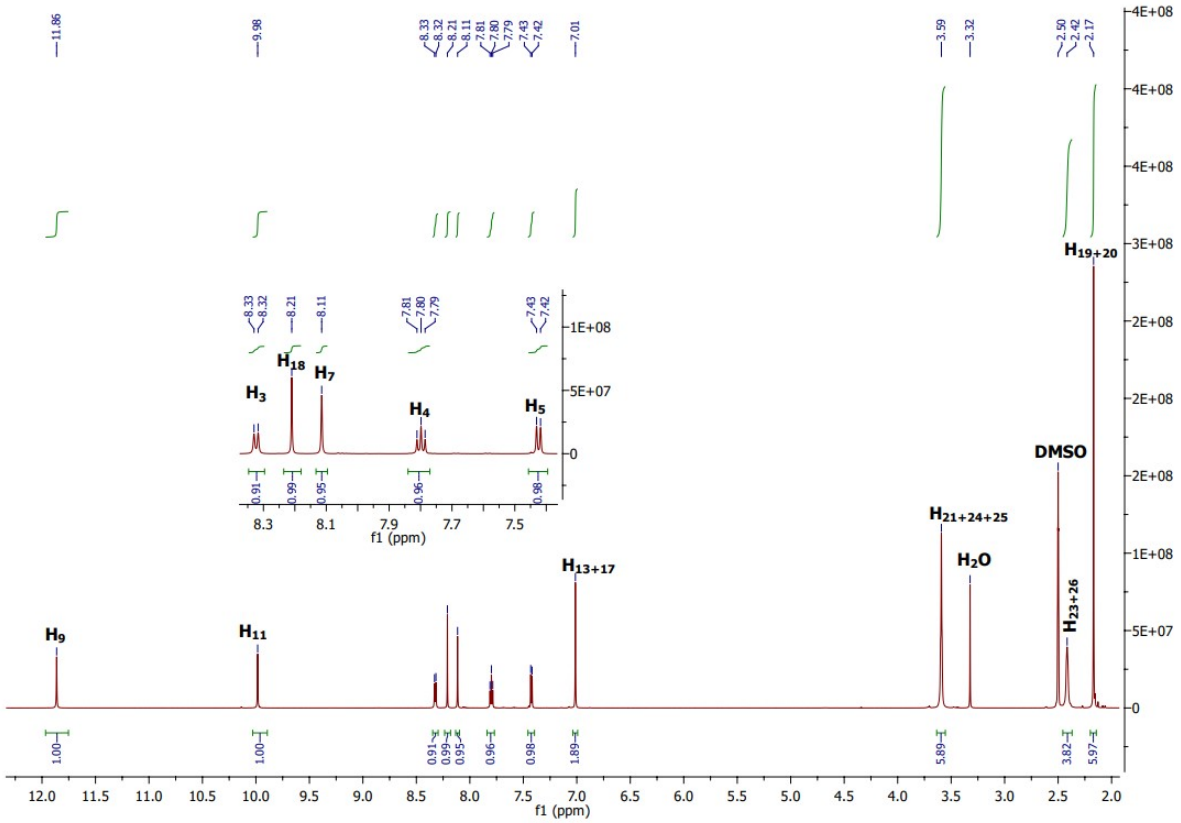

Figure S1A. ^{1}H NMR spectrum of **HL^{1}**.

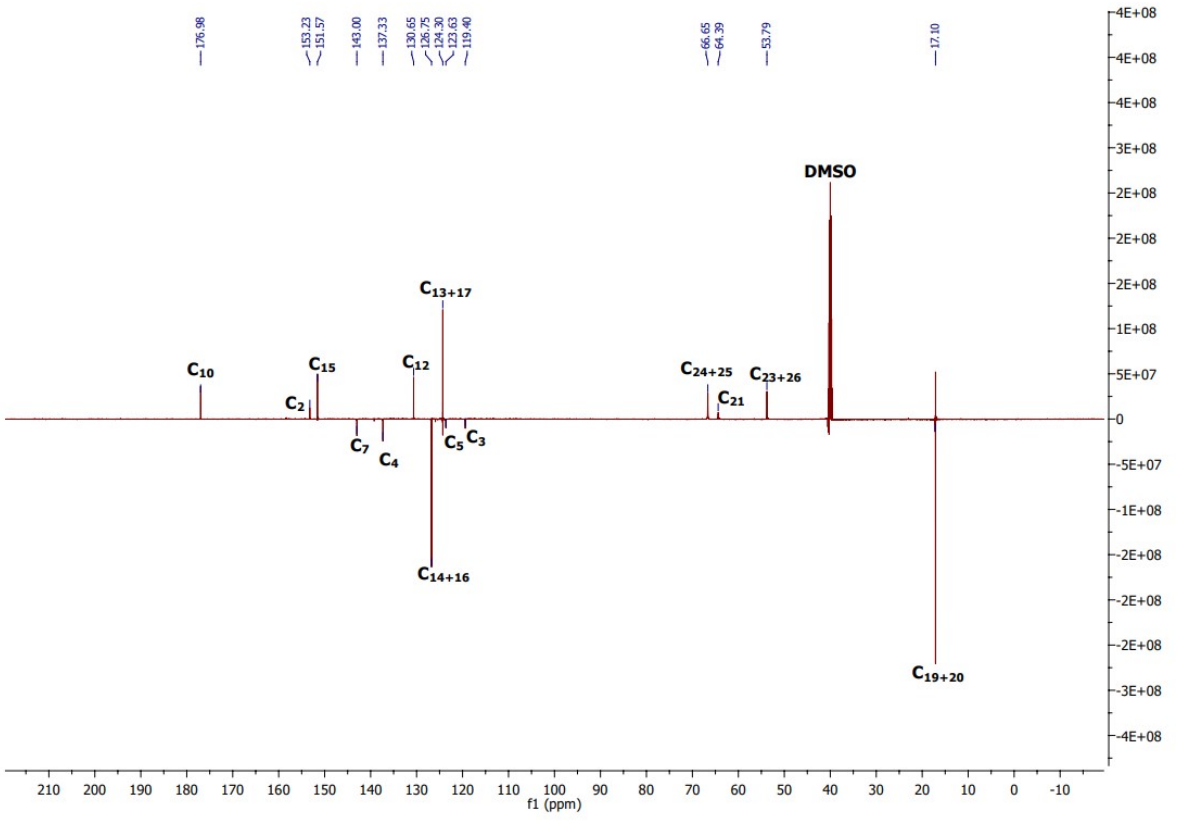

Figure S1B. ^{13}C NMR spectrum of **HL^{1}**.

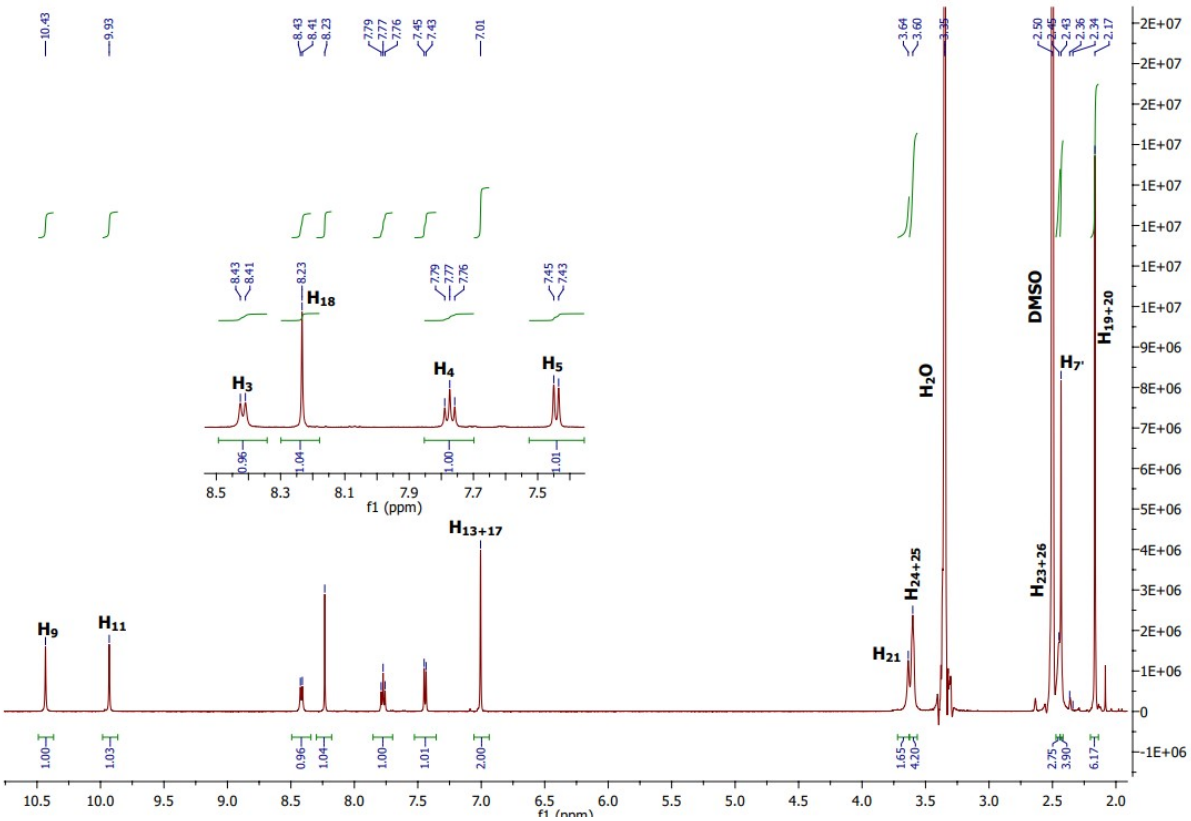

Figure S2A. ^{1}H NMR spectrum of **HL^{2}**.

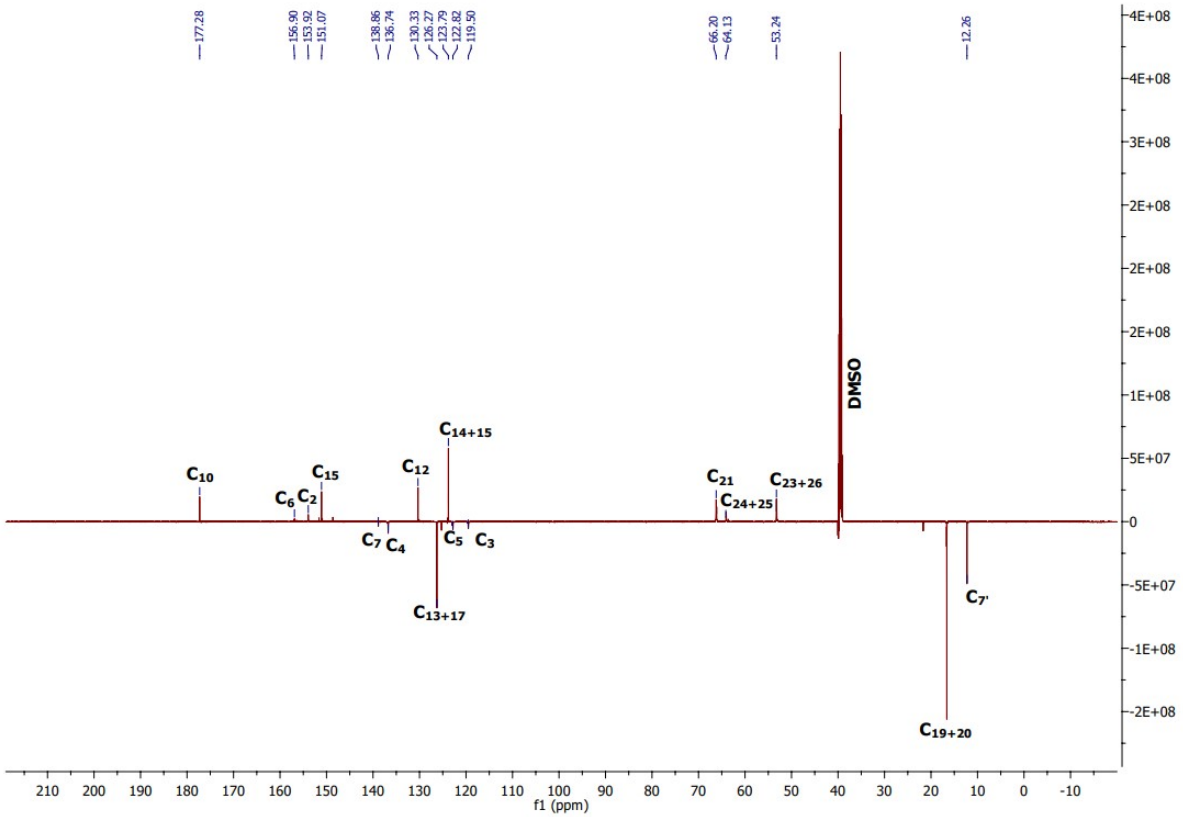

Figure S2B. ^{13}C NMR spectrum of **HL^{2}**.

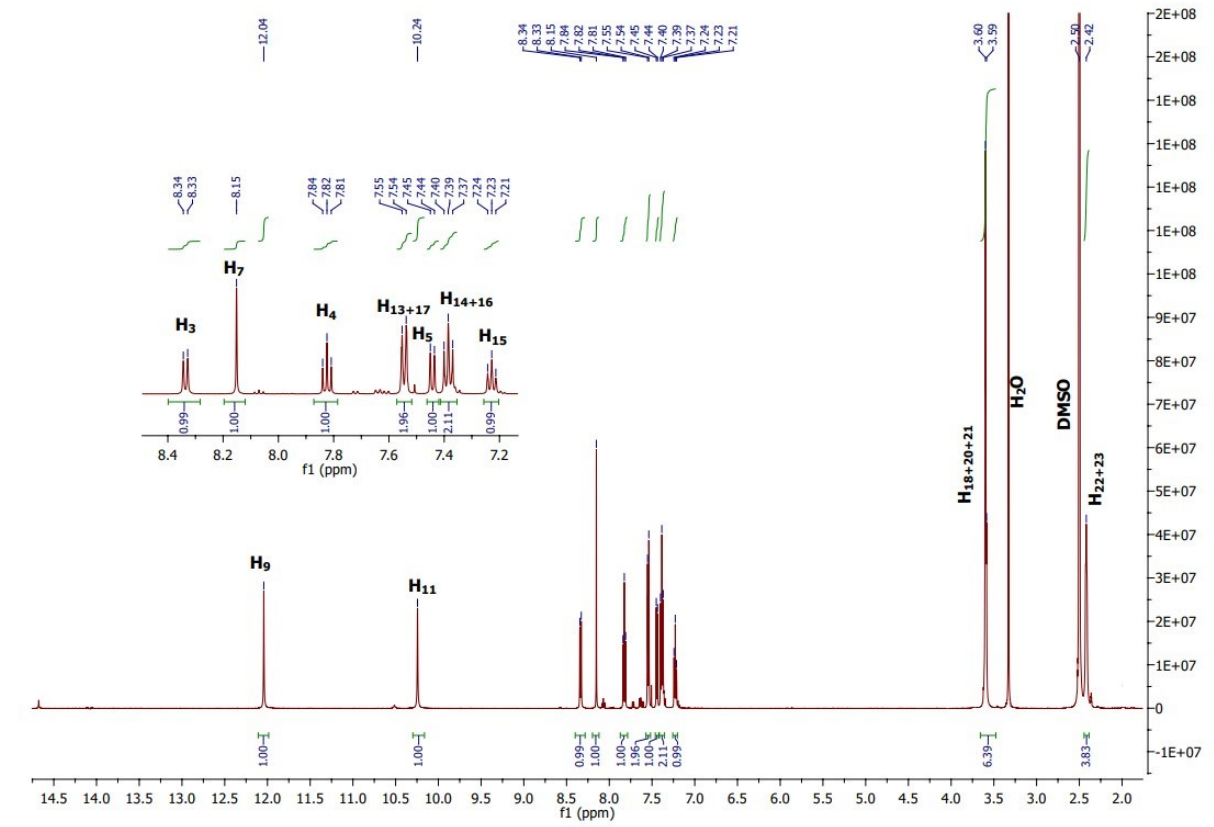

Figure S3A. ^{1}H NMR spectrum of **HL^{3}**.

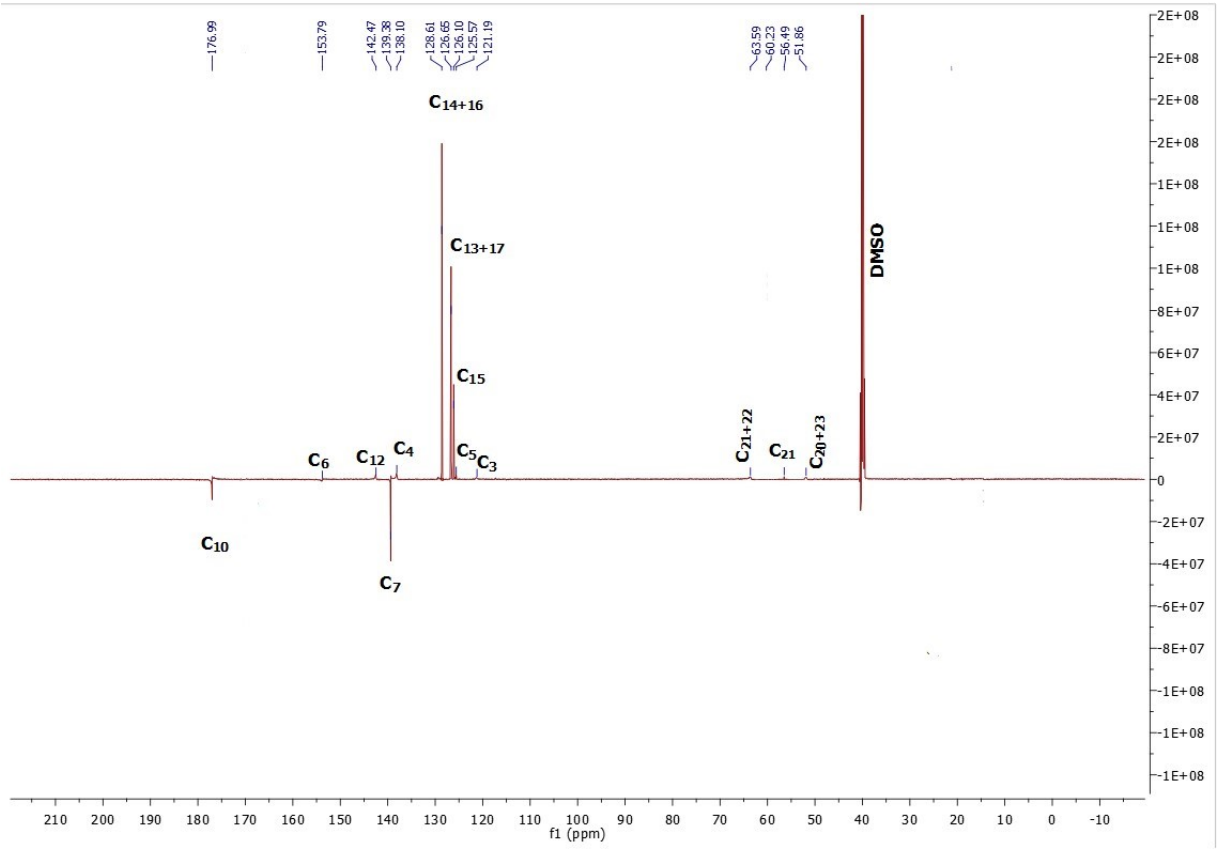

Figure S3B. ^{13}C NMR spectrum of **HL^{3}**.

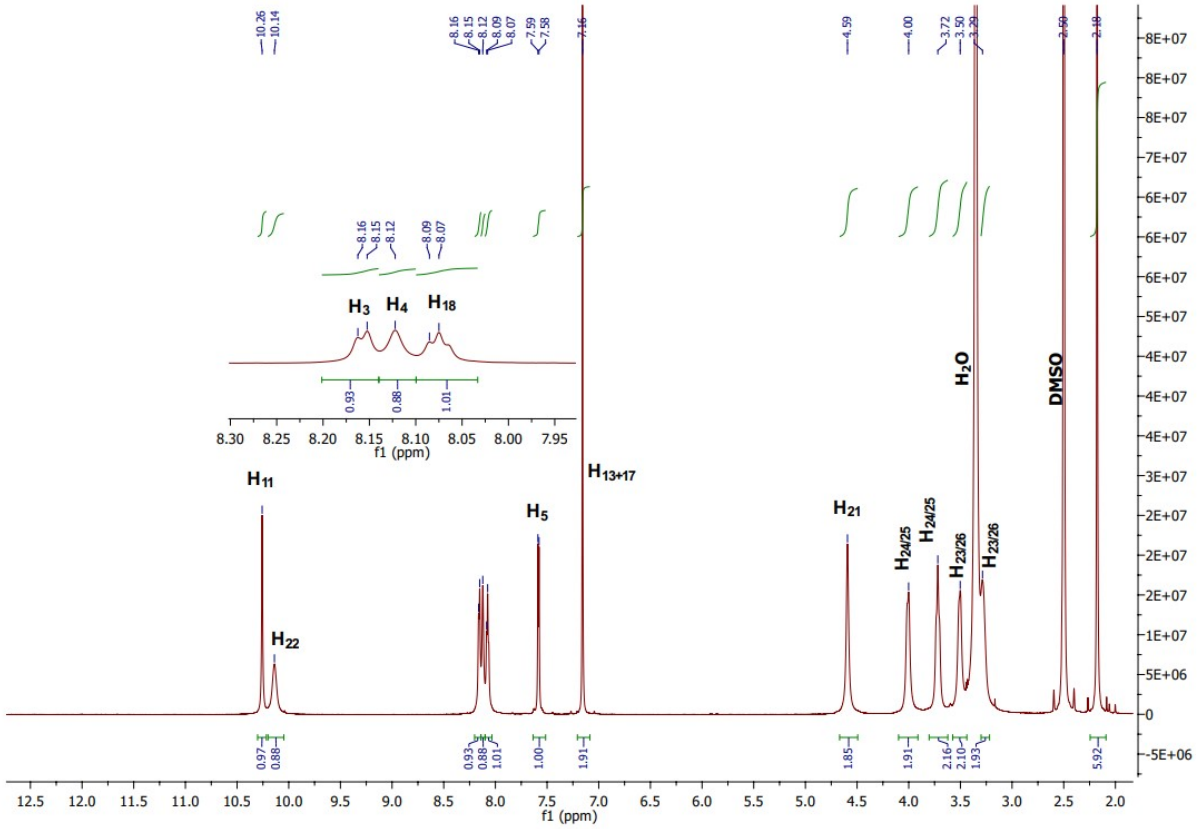

Figure S4A. ^{1}H NMR spectrum of **H*L*$^{1'}$**.

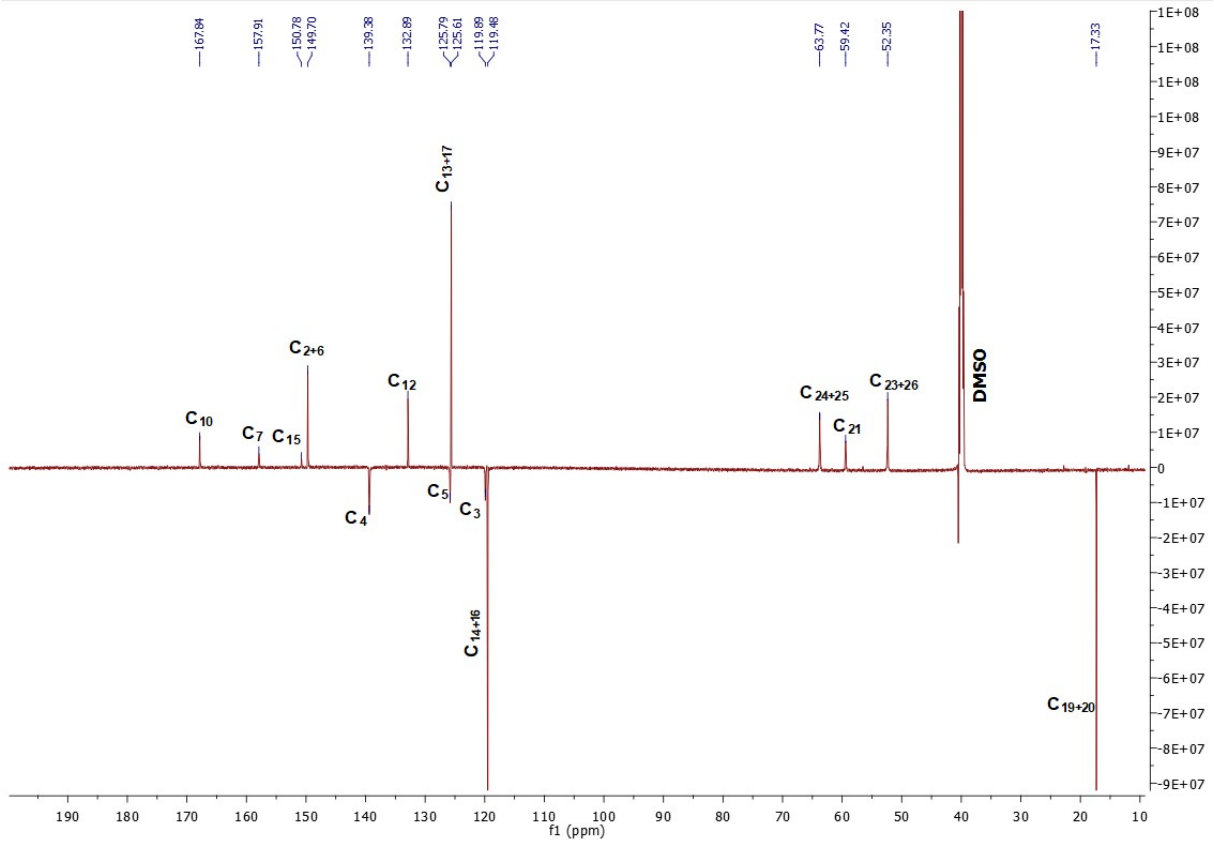

Figure S4B. ^{13}C NMR spectrum of **H*L*$^{1'}$**.

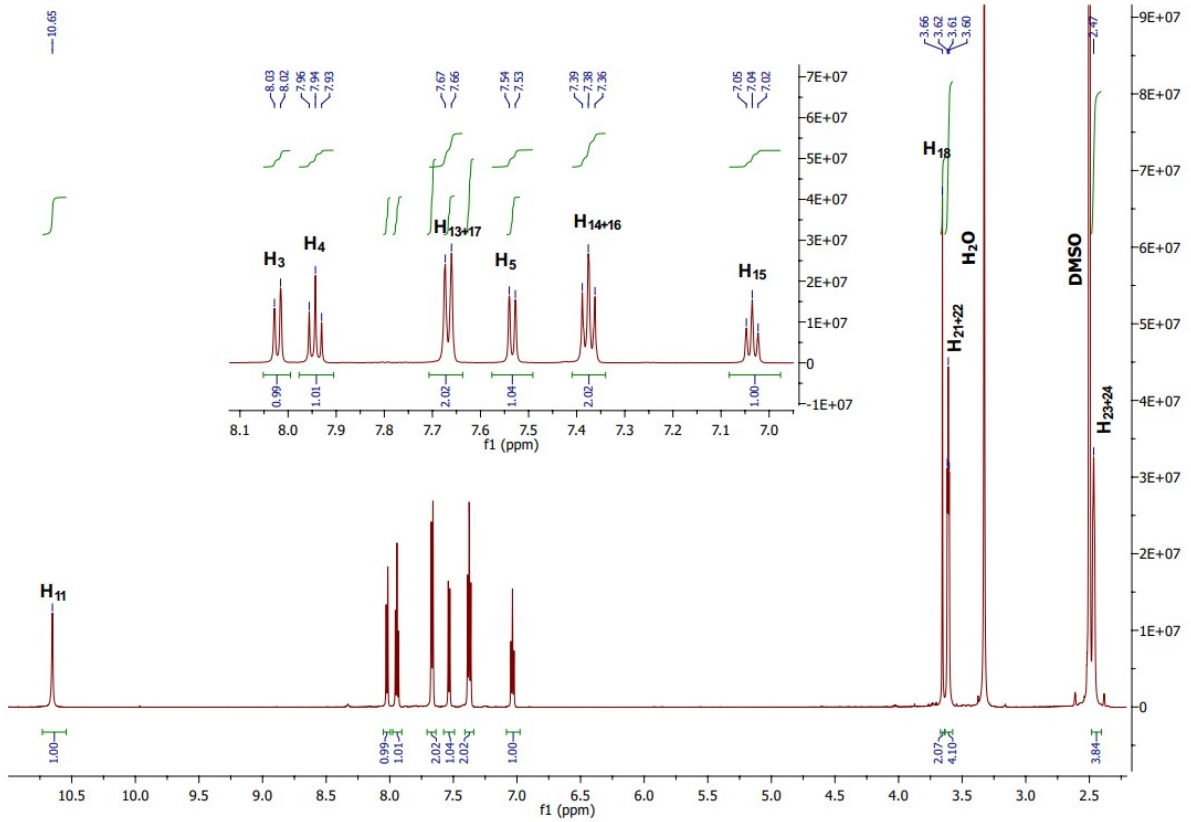

Figure S5A. ^{1}H NMR spectrum of **H*L*$^{3'}$**.

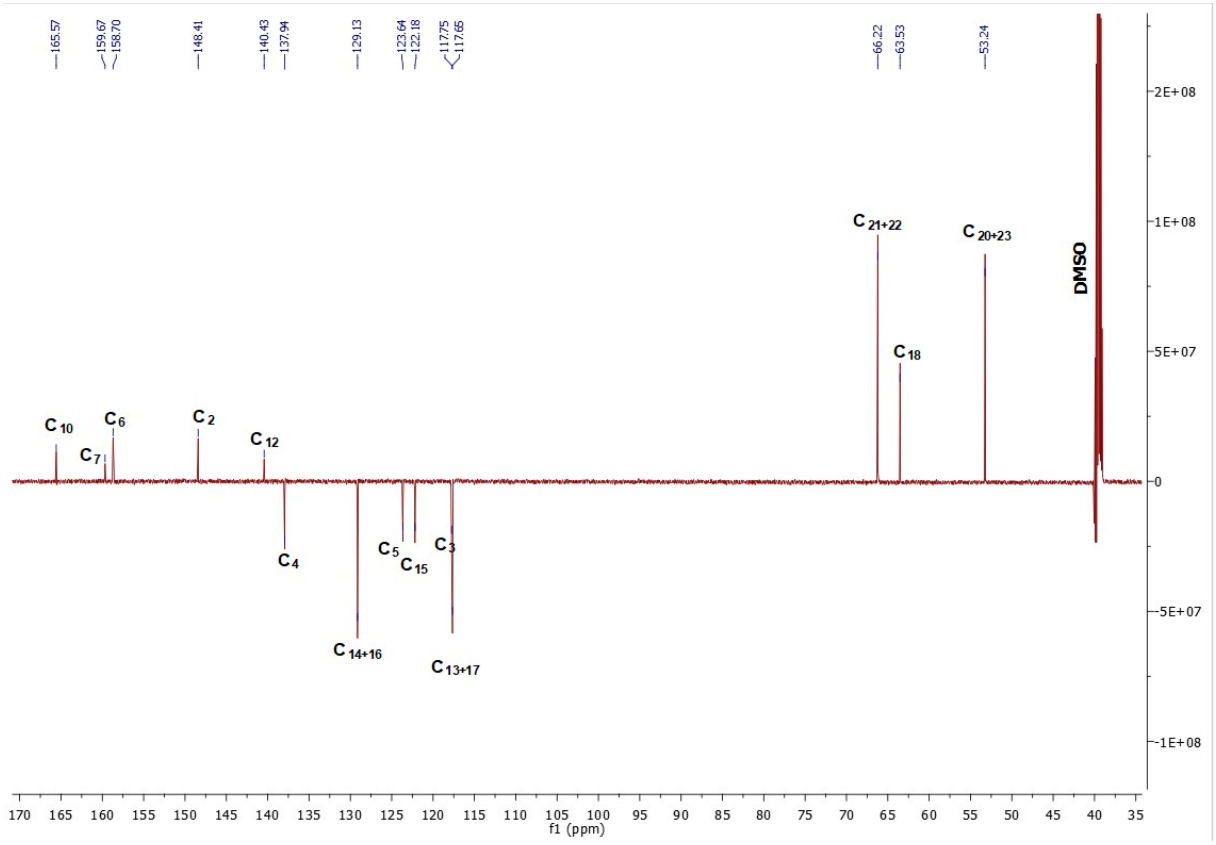

Figure S5B. ^{13}C NMR spectrum of **H*L*$^{3'}$**.

Assignment of proton resonances in ^{1}H NMR spectra of the morp-TSCs (solvent: DMSO-d_6).

		HL^{1} (*E*-)	**H*L*$^{1'}$**	**HL^{2}** (*E*-)	**HL^{3}** (*E*-)	**H*L*$^{3'}$**
H_3	CH_{py}	8.32 (d, 1H)	8.16 (d, 1H)	8.42 (d, 1H)	8.34 (s, 1H)	8.02 (d, 1H)
H_4	CH_{py}	7.80 (t, 1H)	8.08 (d, 1H)	7.77 (t, 1H)	7.82 (s, 1H)	7.95 (d, 1H)
H_5	CH_{py}	7.42 (d, 1H)	7.58 (d, 1H)	7.44 (d, 1H)	7.54 (s, 1H)	7.53 (d, 1H)
H_7	C*H*=N	8.11 (s, 1H)	-	-	8.15 (s, 1H)	-
$H_{7'}$	CH_3(C=N)	-	-	2.45 (s, 3H)	-	-
H_9	N*H* (closer to py)	11.86 (s, 1H)	-	10.43 (s, 1H)	12.04 (s, 1H)	-
H_{11}	N*H* (closer to ph)	9.98 (s, 1H)	10.26 (s, 1H)	9.93 (s, 1H)	10.24 (s, 1H)	10.65 (s, 1H)
H_{13+17}	CH_{ph}	7.01 (s, 2H)	7.16 (s, 2H)	7.01 (s, 2H)	7.44 (d, 2H)	7.67 (d, 2H)
H_{14+16}	CH_{ph}	-	-	-	7.39 (t, 2H)	7.38 (t, 2H)
H_{15}	CH_{ph}	-	-	-	7.23 (t, 1H)	7.04 (s, 1H)
H_{18}	OH_{ph}	8.21 (s, 1H)	8.12 (s, 1H)	8.23 (s, 1H)	-	-
H_{19+20}	CH_3	2.17 (s, 6H)	2.18 (s, 6H)	2.17 (s, 6H)	-	-
H_{22} (H_{19} for **HL^{3}** and **H*L*$^{3'}$**)	N$H_{(morph)}$	-	10.14 (s, 1H	-	11.38 (s, 1H)	-
H_{21} (H_{18} for **HL^{3}** and **H*L*$^{3'}$**)	CH_2–N$_{(morph)}$	3.59 (s, 6H)	4.59 (s, 2H)	3.64 (s, 2H)	3.59 (s, 6H)	3.66 (s, 2H)
H_{24+25} (H_{21+22} for **HL^{3}** and **H*L*$^{3'}$**)	C$H_{2\ (morph)}$ (closer to O)		4.00 (s, 2H) 3.72 (s, 2H)	3.60 (s, 4H)		3.61 (m, 4H)
H_{23+26} (H_{20+23} for **HL^{3}** and **H*L*$^{3'}$**)	C$H_{2\ (morph)}$ (closer to N)	2.42 (s, 4H)	3.50 (s, 2H) 3.29 (s, 2H)	2.43 (s, 4H)	2.42 (s, 4H)	2.47 (s, 4H)

Assignment of ^{13}C resonances in ^{13}C NMR spectra of the morp-TSCs (solvent: DMSO-d_6).

		HL^1 (*E*-)	**H*L*$^{1'}$**	**HL^2** (*E*-)	**HL^3** (*E*-)	**H*L*$^{3'}$**
C_2	C_{py}	153.23	149.67	153.92	149.17*	148.41
C_3	CH_{py}/C_{py}	119.40	119.89	119.50	121.19	117.75
C_4	CH_{py}	137.33	139.38	136.74	138.10	137.94
C_5	CH_{py}	123.63	125.79	122.82	125.57	123.64
C_6	CH_{py}	158.16*	149.70	156.90	153.76	158.70
C_7	C=N	143.00	-	138.86	139.38	-
C_7	thiadiazole	-	157.91	-	-	159.67
$C_{7'}$	CH_3 (C=N)	-	-	12.26	-	-
C_{10}	C=S	176.98	-	177.28	176.99	-
C_{10}	S-C-N	-	167.84	-	-	165.57
C_{12}	C_{ph}	130.65	132.89	130.33	142.47	140.43
C_{13+17}	CH_{ph}	126.75	119.48	126.27	126.65	117.65
C_{14+16}	$C(CH_3)_{ph}$	124.30	125.61	123.79	128.61	129.13
C_{15}	$C(OH)_{ph}$	151.57	150.77	151.07	126.10	122.18
C_{19+20}	$C(CH_3)_{ph}$	17.10	17.33	16.60	-	-
C_{21} (C_{18} for **HL^3** and **H*L*$^{3'}$**)	CH_2–$N_{(morph)}$	64.39	59.42	66.20	60.23	63.53
C_{24+25} (C_{21+22} for **HL^3** and **H*L*$^{3'}$**)	$CH_{2\ (morph)}$ (closer to O)	66.65	63.77	64.13	63.59	66.22
C_{23+26} (C_{20+23} for **HL^3** and **H*L*$^{3'}$**)	$CH_{2\ (morph)}$ (closer to N)	53.79	52.35	53.24	51.86	53.24

*Resonances were assigned by using ^1H–^{13}C HSQC, ^1H–^{13}C HMBC and ^1H–^1H COSY NMR spectra.

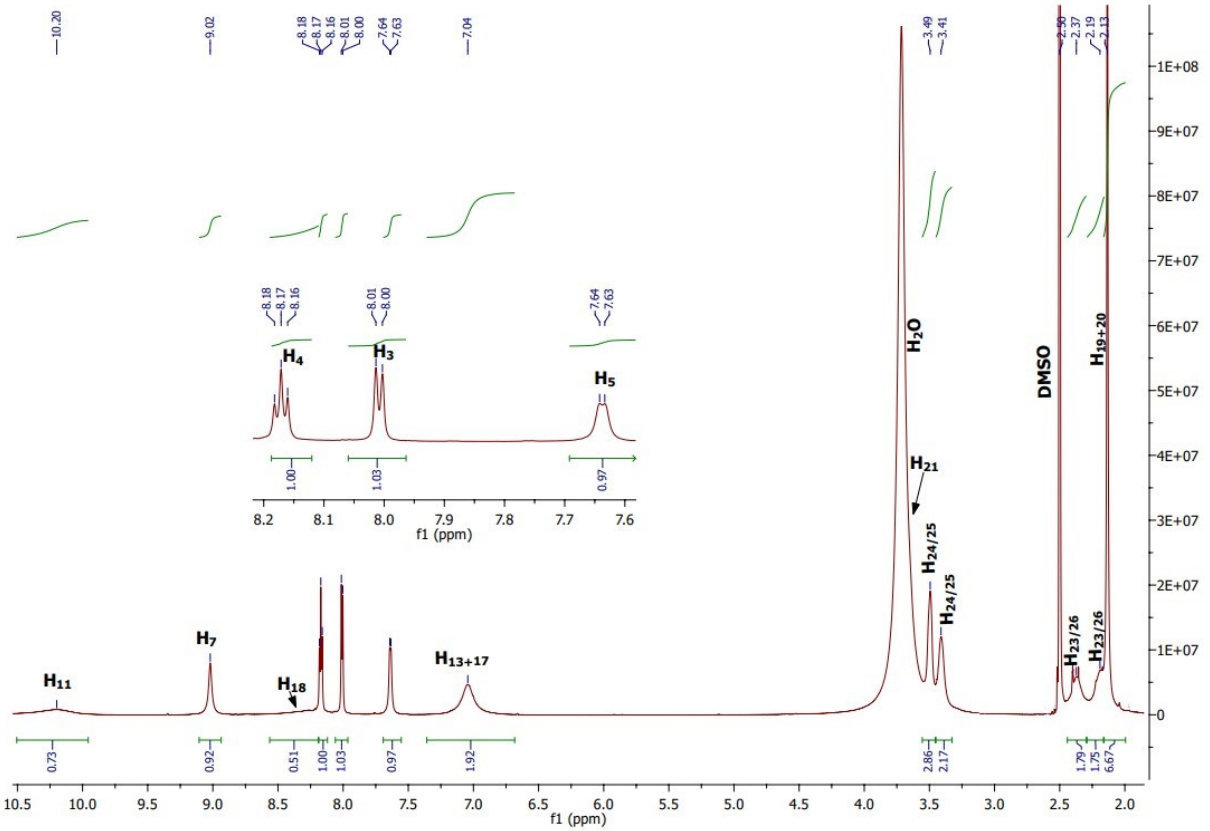

Figure S6A. ^{1}H NMR spectrum of **1**.

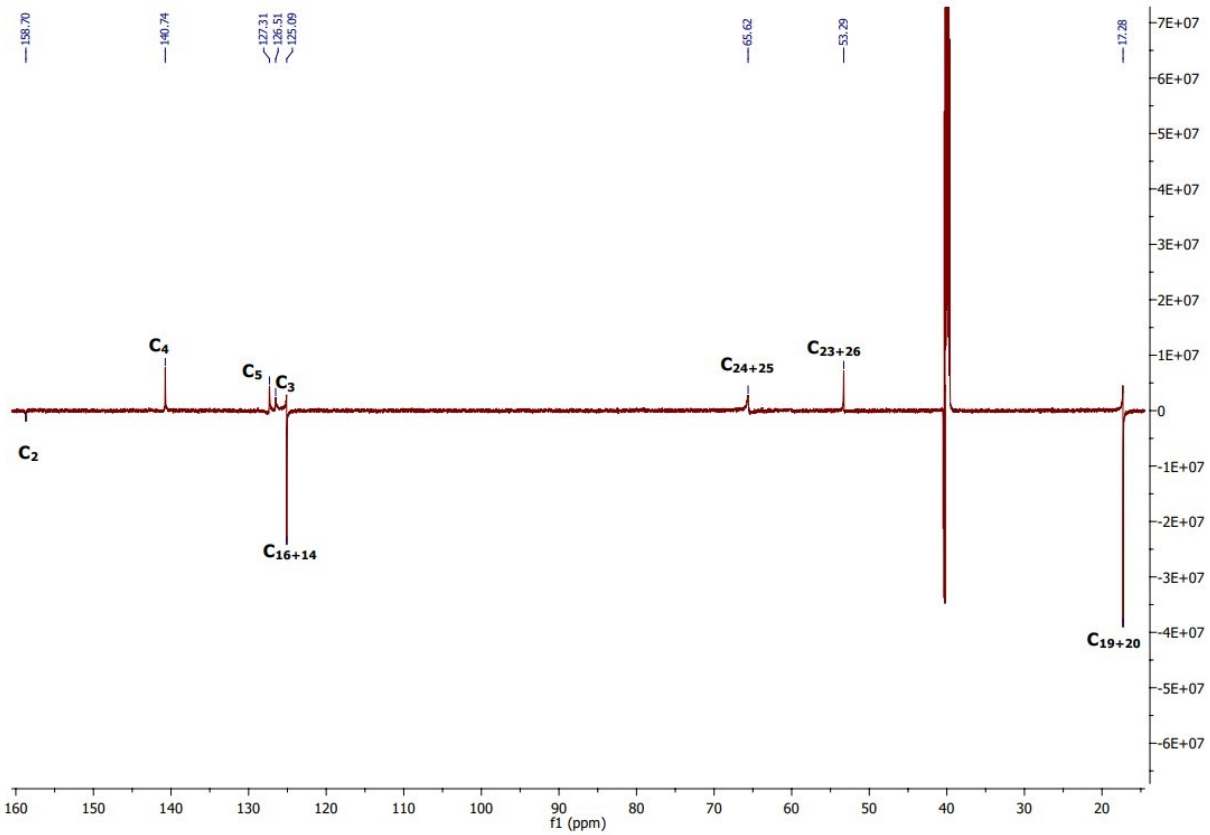

Figure S6B. ^{13}C NMR spectrum of **1**.

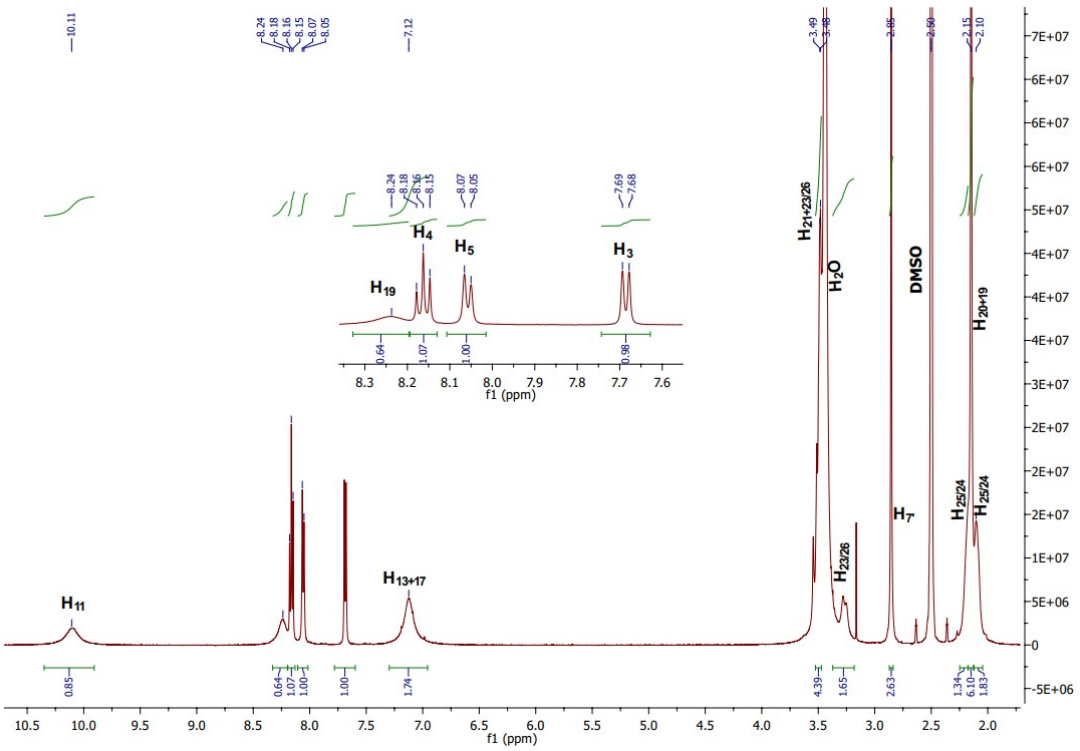

Figure S7A. ^{1}H NMR spectrum of **2.**

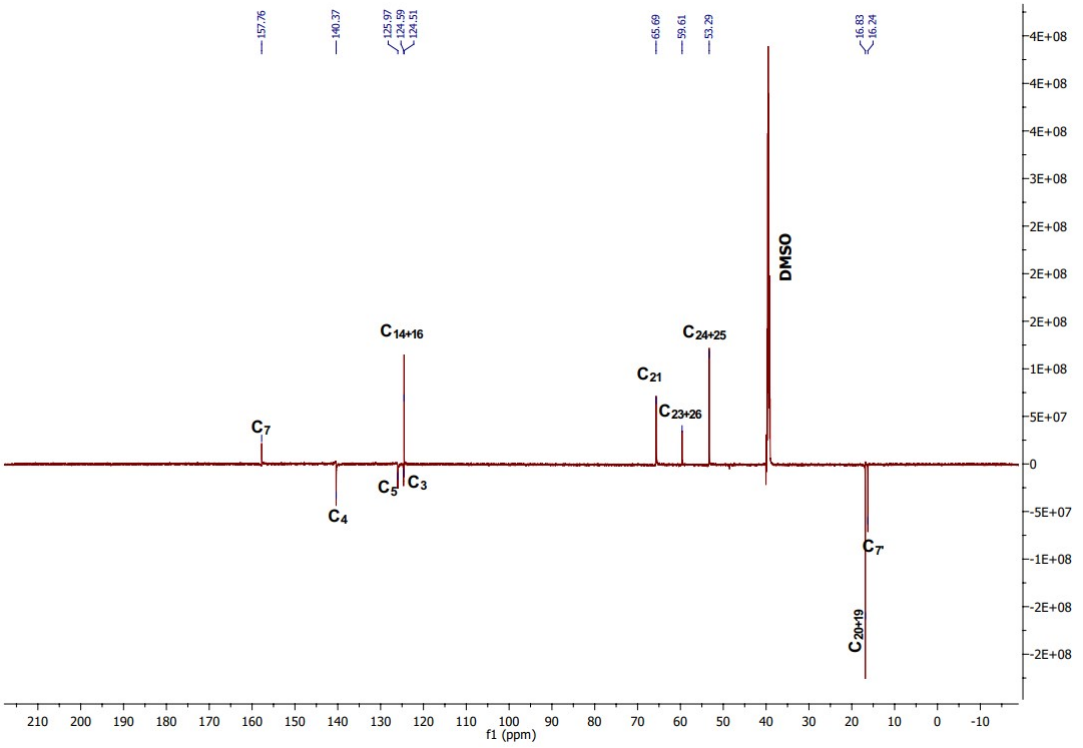

Figure S7B. ^{13}C NMR spectrum of **2.**

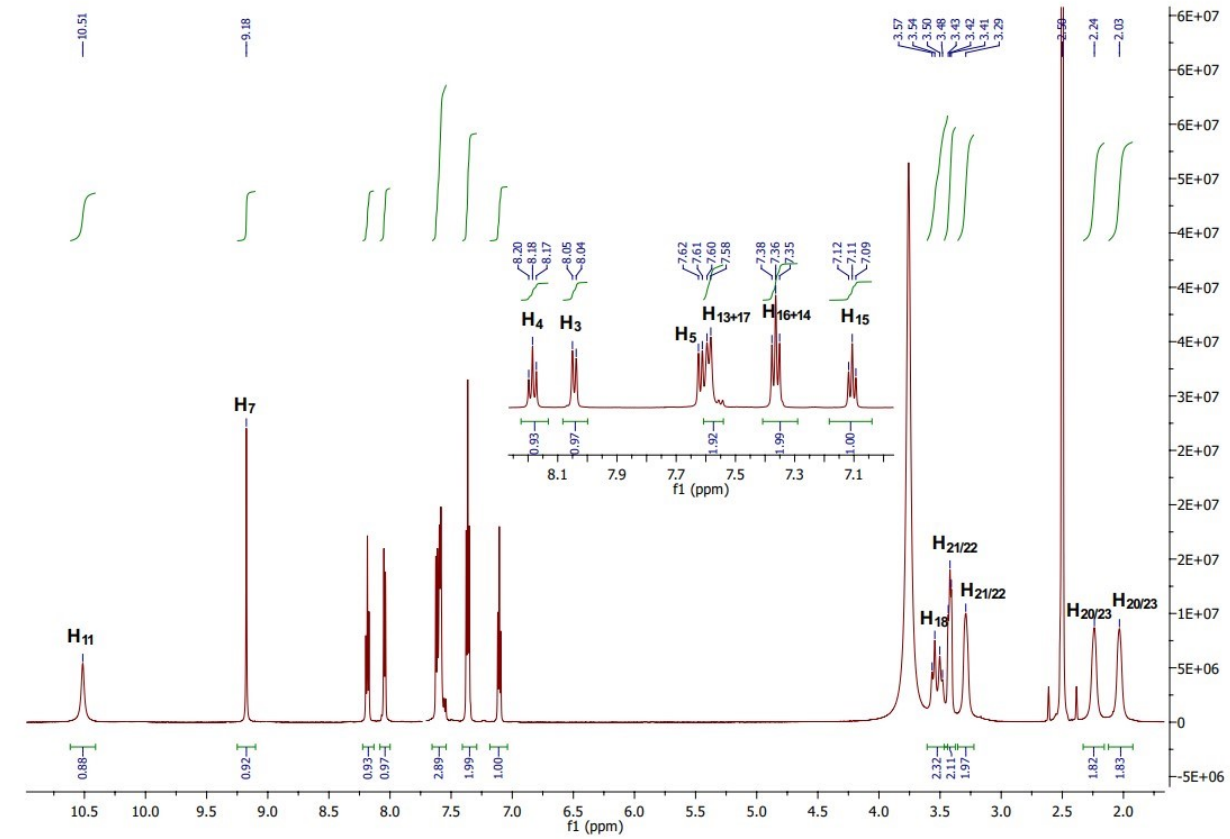

Figure S8A. ^{1}H NMR spectrum of **3.**

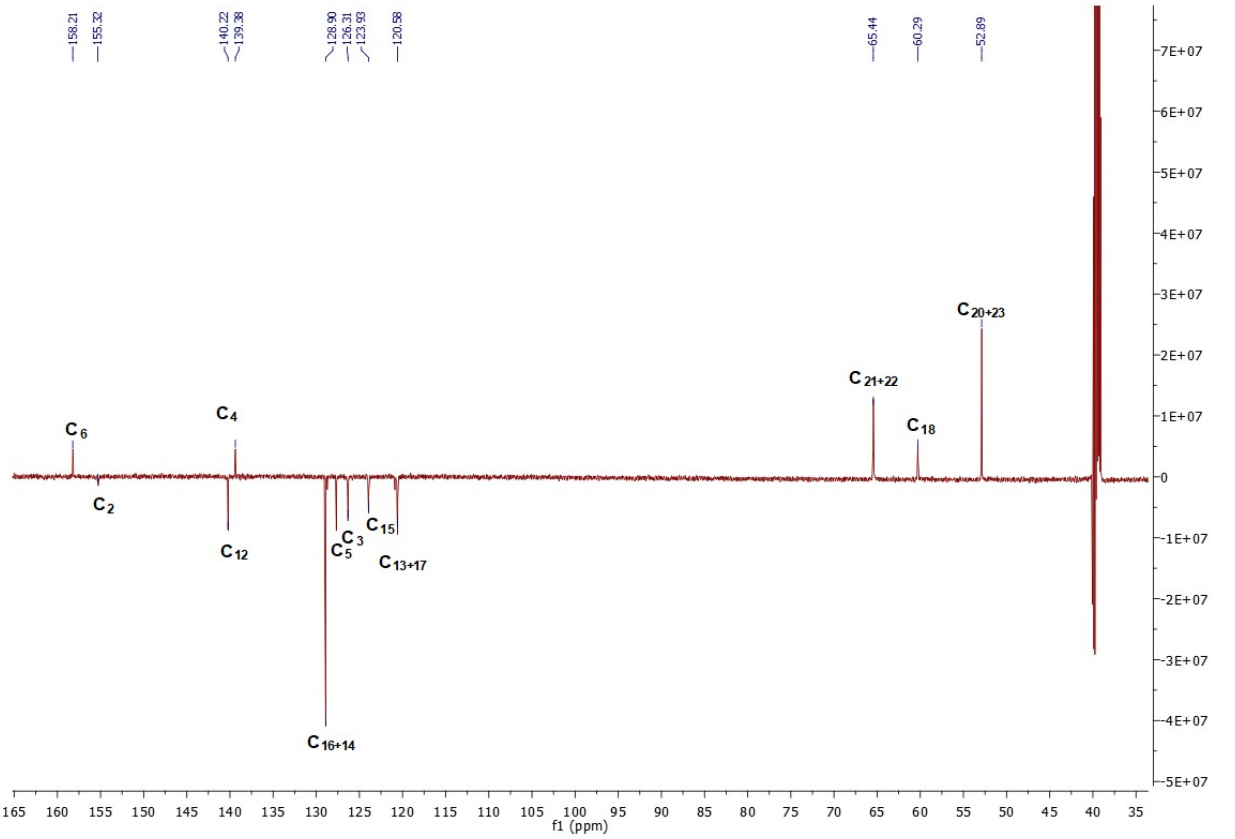

Figure S8B. ^{13}C NMR spectrum of **3**.

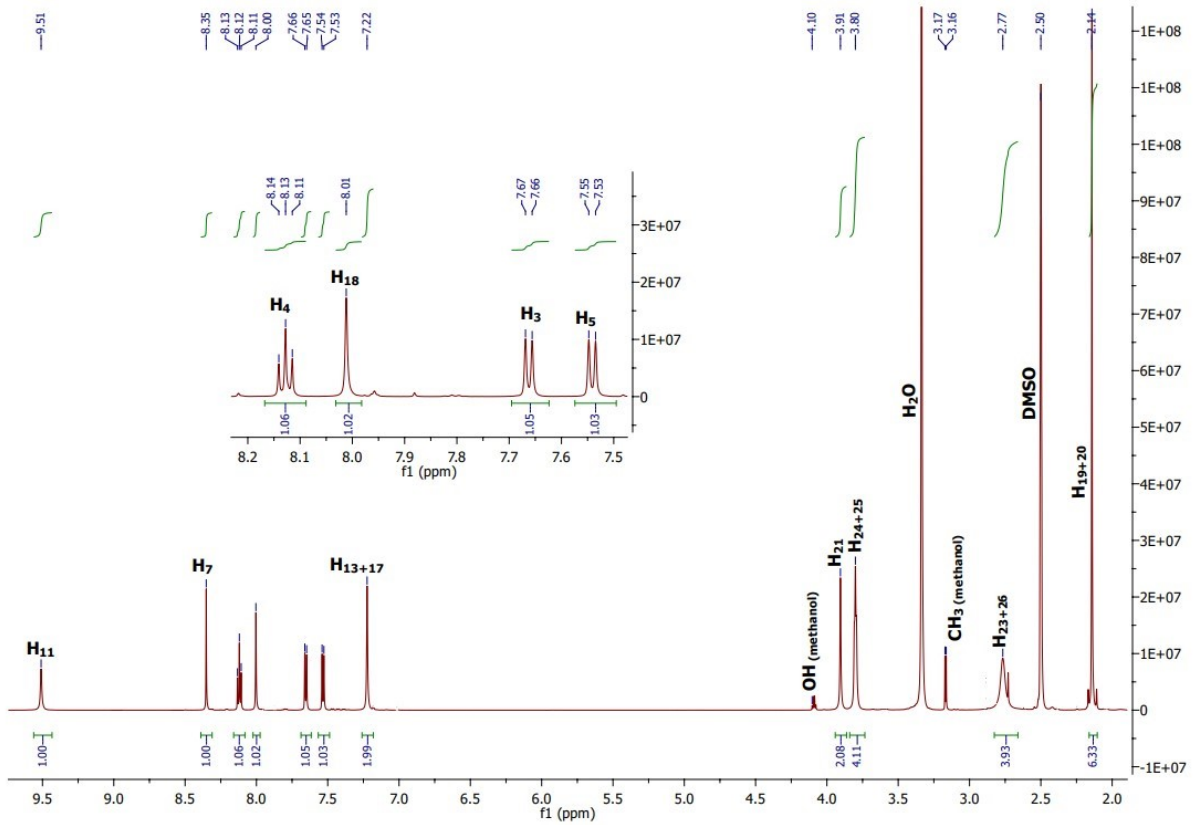

Figure S9A. ^{1}H NMR spectrum of **7**.

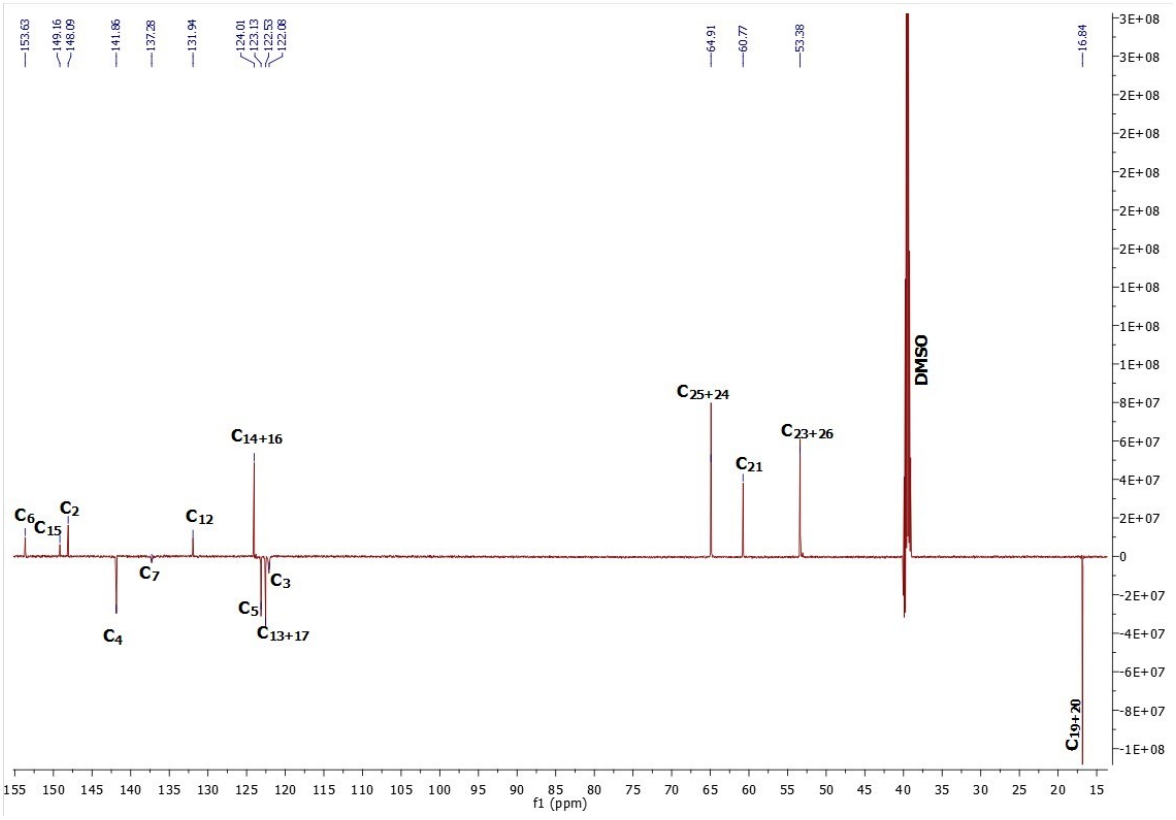

Figure S9B. ^{13}C NMR spectrum of **7**.

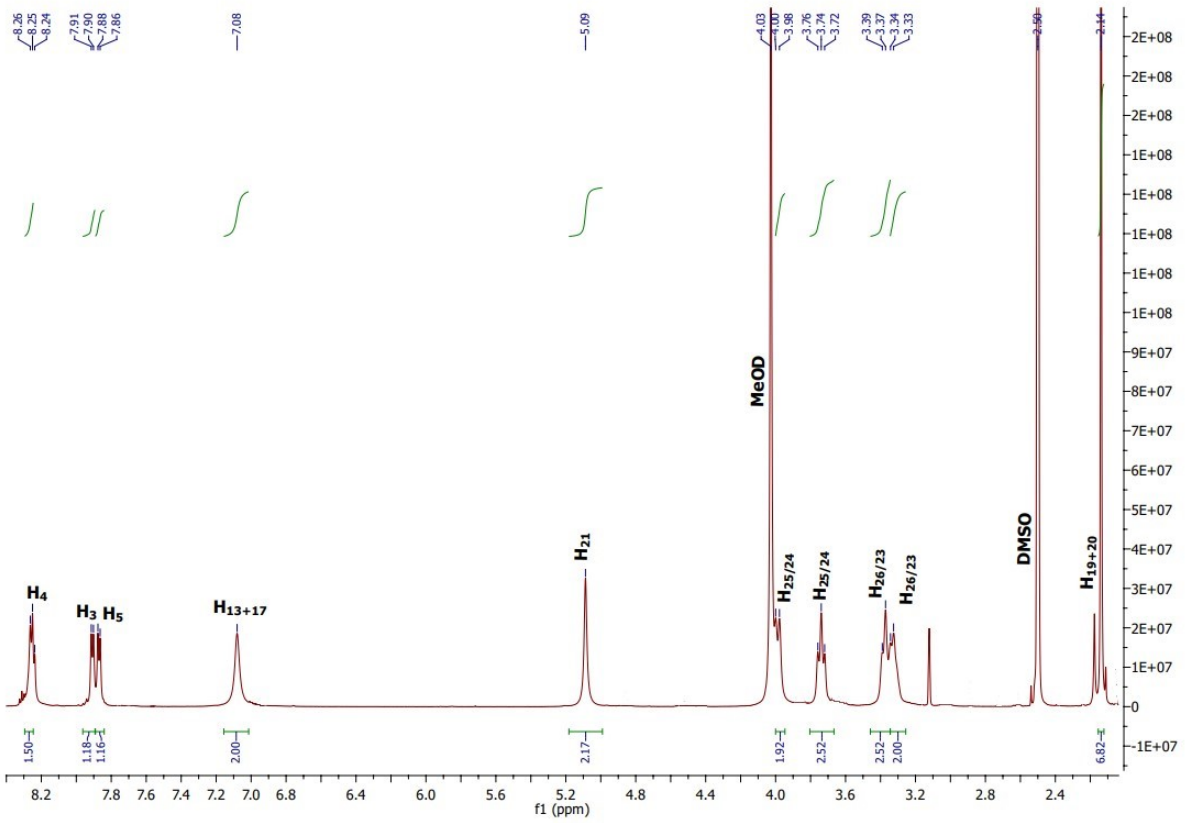

Figure S10A. ^{1}H NMR spectrum of **8**.

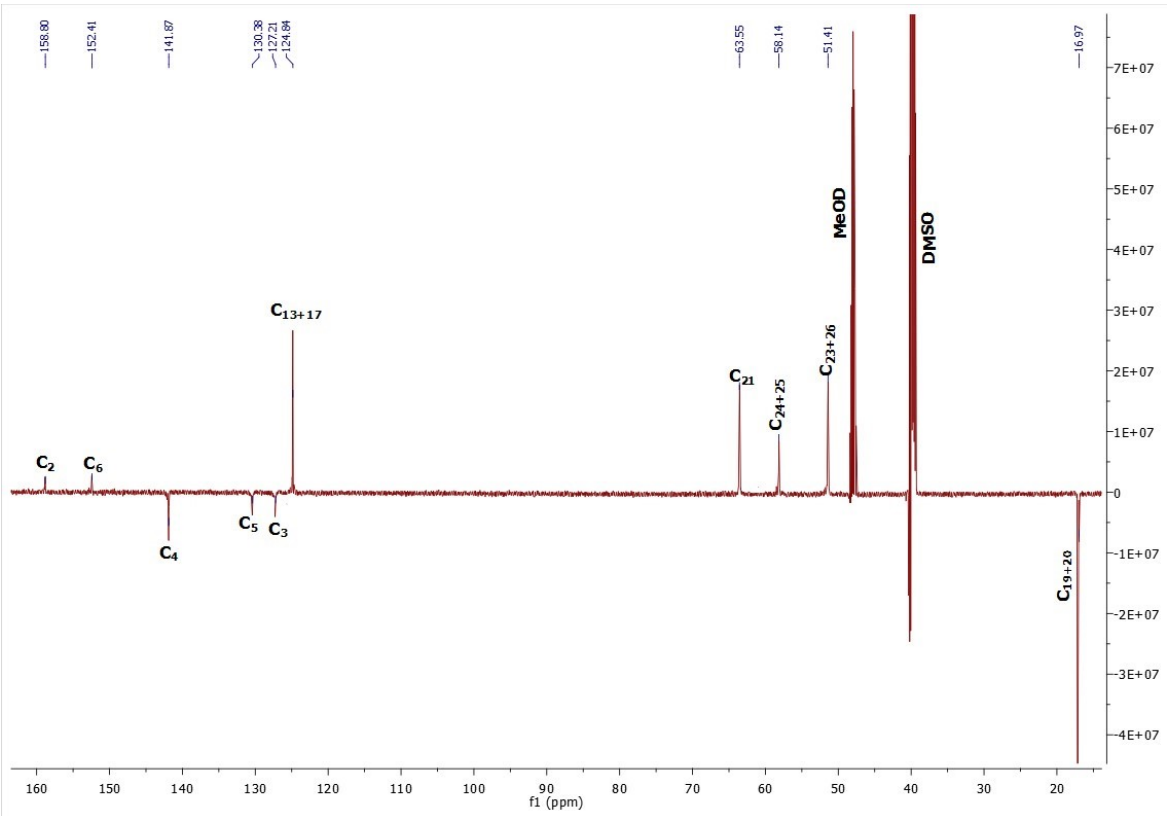

Figure S10B. ^{13}C NMR spectrum of **8**.

Assignment of proton resonances in ^{1}H NMR spectra of **1**, **7** and **8** (solvent: DMSO-d_6).

		HL[1] (*E*-)	**1**	**7**	**8***
H_3	CH_{py}	8.32 (d, 1H)	8.01 (d, 1H)	7.66 (d, 1H)	7.91 (d, *1*H)
H_4	CH_{py}	7.80 (t, 1H)	8.17 (t, 1H)	8.13 (t, 1H)	8.26 (t, 1H)
H_5	CH_{py}	7.42 (d, 1H)	7.64 (d, 1H)	7.54 (d, 1H)	7.87 (d, *1*H)
H_7	C*H*=N	8.11 (s, 1H)	9.02 (s, 1H)	8.36 (s, 1H)	not detected
H_9	N*H* (closer to py)	11.86 (s, 1H)	-	-	-
H_{11}	N*H* (closer to ph)	9.98 (s, 1H)	10.20 (s, 1H)	9.52 (s, 1H)	not detected
H_{13+17}	CH_{ph}	7.01 (s, 2H)	7.04 (b, 2H)	7.23 (s, 2H	7.08 (s, 2H)
H_{18}	OH_{ph}	8.21 (s, 1H)	8.56 – 8.19 (b, 1H)	8.01 (s, 1H)	not detected
H_{19+20}	CH_{3ph}	2.17 (s, 6H)	2.13 (s, 6H)	2.15 (s, 6H)	2.14 (s, 6H)
H_{22}	N$H_{(morph)}$	-	-	-	-
H_{21}	CH_2 –N$_{(morph)}$	3.59 (s, 6H)	3.69 (s, 4H)* + ($H_{24/25}$)	3.91 (s, 2H)	5.09 (s, 2H)
H_{24+25}	C$H_{2\ morph}$ (closer to O)		3.49 (s, 2H) 3.41 (s, 2H)	3.81 (s, 4H)	3.98 (m, 1H) 3.74 (m, 1H)
H_{23+26}	C$H_{2\ morph}$ (closer to N)	2.42 (s, 4H)	2.37 (s, 2H) 2.19 (s, 2H)	2.77 (s, 4H)	3.37 (m, 1H) 3.33 (m, 1H)

*Measured in DMSO-d_6 + 10% MeOD-d_4.

Assignment of ^{13}C resonances in ^{13}C NMR spectra of **1**, **7** and **8** (solvent: DMSO-d_6).

		HL[1] (*E*-)	**1**	**7**	**8***
C_2	C_{py}	153.23	158.70	148.09	158.80
C_3	CH_{py}/C_{py}	119.40	126.51	122.53	127.21
C_4	CH_{py}	137.33	140.74	141.86	141.87
C_5	CH_{py}	123.63	127.31	123.13	130.38
C_6	CH_{py}	158.16	not detected	153.63	152.41
C_7	*C*=N	143.00	not detected	137.28	not detected
C_{10}	*C*=S	176.98	-	-	-
C_{10}	S-*C*-N	-	not detected	not detected	not detected
C_{12}	C_{ph}	130.65	not detected	131.94	not detected
C_{13+17}	CH_{ph}	126.75	not detected	122.08	124.84
C_{14+16}	$C(CH_3)_{ph}$	124.30	125.09	124.01	not detected
C_{15}	$C(OH)_{ph}$	151.57	151.04*	149.16	not detected
C_{19+20}	$C(CH_3)_{ph}$	17.10	17.28	16.84	16.97
C_{21}	CH_2–$N_{(morph)}$	64.39	60.06*	60.77	63.55
C_{24+25}	$CH_{2\ (morph)}$ (closer to O)	66.65	65.62	64.91	58.14
C_{23+26}	$CH_{2\ (morph)}$ (closer to N)	53.79	53.29	53.38	51.41

*Resonances were assigned by using ^1H–^{13}C HSQC, ^1H–^{13}C HMBC and ^1H–^1H COSY NMR spectra.

2. Crystallographic data collection

Table S1. Crystal Data and Details of Data Collection and Refinement for $[Co^{III}(HL^1)(L^1)](NO_3)_2 \cdot H_2O$ **(1)**, $[Co^{III}(HL^3)(L^3)](NO_3)_2$**(3),** $[Fe^{III}(L^2)_2]NO_3$ (**4**), $[Fe^{III}(HL^3)(L^3)](NO_3)_2$ (**6**).

compound	$[Co^{III}(HL^1)(L^1)](NO_3)_2 \cdot H_2O$	$[Co^{III}(HL^3)(L^3)](NO_3)_2$	$[Fe^{III}(L^2)_2]NO_3$	$[Fe^{III}(HL^3)(L^3)](NO_3)_2$
empirical formula	$C_{40}H_{51}CoN_{12}O_{11}S_2$	$C_{38}H_{49}CoN_{12}O_{10}S_2$	$C_{42.65}H_{54.60}FeN_{11}O_{7.65}S_2$	$C_{36}H_{41}FeN_{12}O_8S_2$
fw	998.97	956.94	963.74	889.78
space group	$P2_1/c$	$P2_1/n$	$P2_1/n$	$P2_1/n$
a, Å	19.607(3)	17.659(4)	16.8583(16)	17.7730(5)
b, Å	17.3104(15)	9.9034(13)	13.8926(7)	9.9333(2)
c, Å	15.5505(15)	24.975(7)	21.7744(17)	24.8488(7)
α, °				
β, °	109.389(10)	95.42(2)	107.706(7)	95.264(2)
γ, °				
V [Å^3]	4978.7(11)	4348.1(17)	4858.1(7)	4368.4(2)
Z	4	4	4	4
λ [Å]	0.71073	0.71073	0.71073	0.71073
ρ_{calcd}, g cm^{-3}	1.333	1.462	1.318	1.353
cryst size, mm^3	0.17 × 0.11 × 0.04	0.25 × 0.12 × 0.03	0.20 × 0.12 × 0.01	0.30 × 0.14 × 0.02
T [K]	100(2)	100(2)	100(2)	100(2)
μ, mm^{-1}	0.495	0.561	0.456	0.503
R_1[a]	0.0526	0.0416	0.0851	0.0325
wR_2[b]	0.1289	0.1053	0.2308	0.0762
GOF[c]	0.918	0.929	0.953	0.945
CCDC no.	2354137	2354138	2354139	2354140

[a] $R_1 = \Sigma||F_o| - |F_c||/\Sigma|F_o|$. [b] $wR_2 = \{\Sigma[w(F_o^2 - F_c^2)^2]/\Sigma[w(F_o^2)^2]\}^{1/2}$. [c] $GOF = \{\Sigma[w(F_o^2 - F_c^2)^2]/(n - p)\}^{1/2}$, where n is the number of reflections and p is the total number of parameters refined.

Table S2. Crystal Data and Details of Data Collection and Refinement for $[Ni^{II}(L^1)]Cl \cdot CH_3OH$, $[Zn^{II}(L^1)Cl] \cdot CH_3OH$ and $[Pd^{II}(HL^1)Cl]Cl$

compound	$[Ni^{II}(L^1)]Cl\cdot CH_3OH$	$[Zn^{II}(L^1)Cl]\cdot CH_3OH$	$[Pd^{II}(HL^1)Cl]Cl$	$[H_2L^1]NO_3$
empirical formula	$C_{21}H_{28}ClN_5NiO_3S$	$C_{20}H_{24}ClN_5O_2SZn$	$C_{20}H_{27}Cl_2N_5O_3PdS$	$C_{20}H_{24}N_6O_5S$
fw	524.70	499.32	576.81	460.51
space group	*Pnn*2	$P\bar{1}$	*I*2/*c*	$P2_1/n$
a, Å	20.022(3)	9.5512(16)	13.9557(12)	13.9111(13)
b, Å	8.8256(10)	9.8642(17)	15.1993(13)	8.5430(6)
c, Å	17.135(2)	12.120(2)	24.0558(18)	18.0419(18)
α, °		87.313(14)		
β, °		80.712(13)	102.430(5)	92.547(8)
γ, °		70.063(12)		
V [Å^3]	3027.9(7)	1059.3(3)	4983.0(7)	2142.0(3)
Z	4	2	8	4
λ [Å]	0.71073	0.71073	0.71073	1.54178
ρ_{calcd}, g cm^{-3}	1.151	1.565	1.538	1.428
cryst size, mm^3	0.70 × 0.075 × 0.075	0.20 × 0.08 × 0.035	0.13 × 0.08 × 0.02	0.30 × 0.14 × 0.02
T [K]	296(2)	100(2)	100(2)	100(2)
μ, mm^{-1}	0.824	1.412	1.069	1.744
R_1[a]	0.0301	0.0565	0.0369	0.0700
wR_2[b]	0.0603	0.1678	0.0687	0.2007
GOF[c]	1.022	1.088	0.854	0.985
CCDC no.	2354141	2354142	2354143	2354144

[a] $R_1 = \Sigma||F_o| - |F_c||/\Sigma|F_o|$. [b] $wR_2 = \{\Sigma[w(F_o^2 - F_c^2)^2]/\Sigma[w(F_o^2)^2]\}^{1/2}$. [c] GOF = $\{\Sigma[w(F_o^2 - F_c^2)^2]/(n - p)\}^{1/2}$, where *n* is the number of reflections and *p* is the total number of parameters refined.

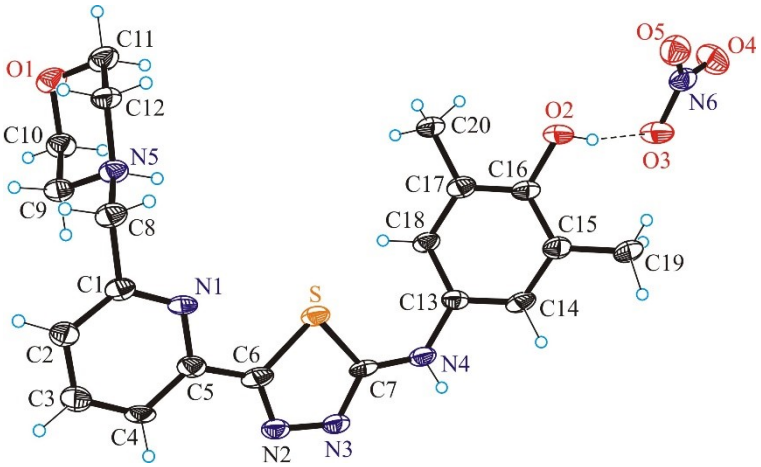

Figure S11. ORTEP view of $[H_2L^1]NO_3$

3. Solution Stability Studies

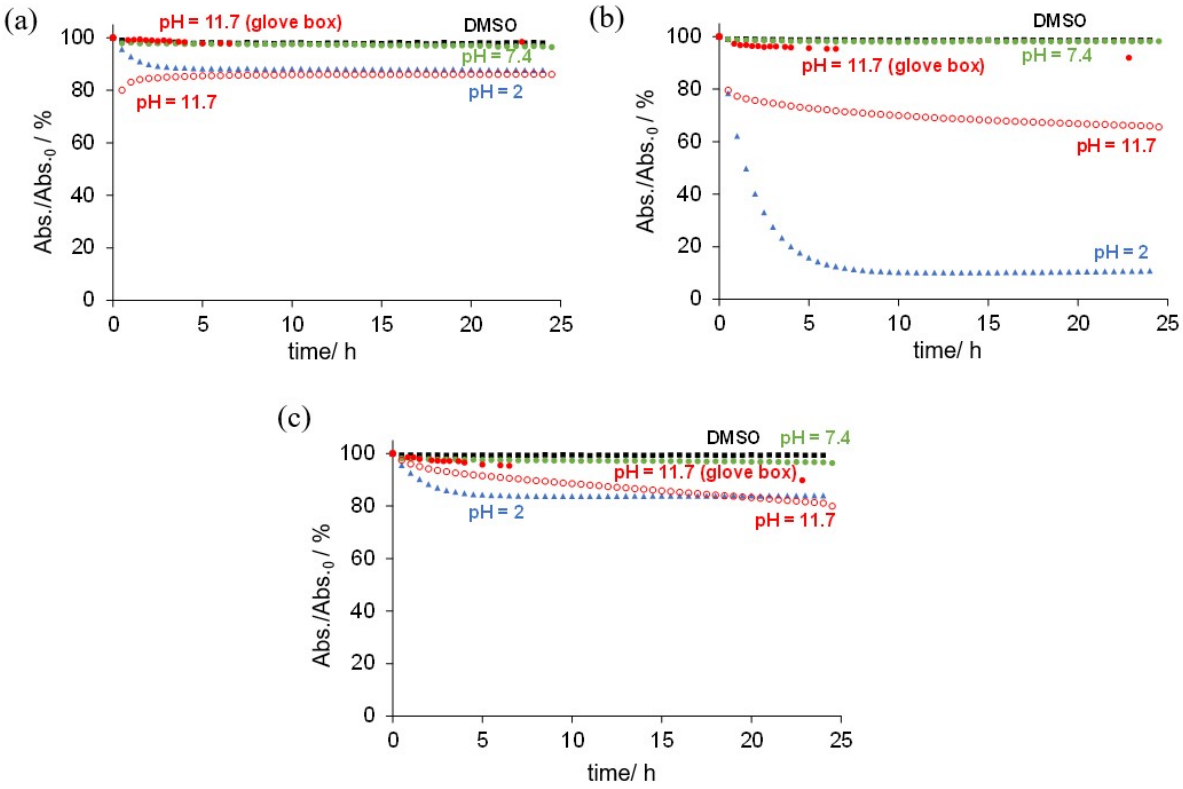

Figure S12. Changes of absorbance values measured for (a) **HL¹**, (b) **HL²** and (c) **HL³** in DMSO (■), at pH 2 (▲), at pH 7.4 (●), at pH 11.7 in glove box (●) and in a normal cuvette (○) over time at the absorbance maximum; {c_{ligand} = 50 μM; ℓ = 1 cm; t = 25.0 °C}.

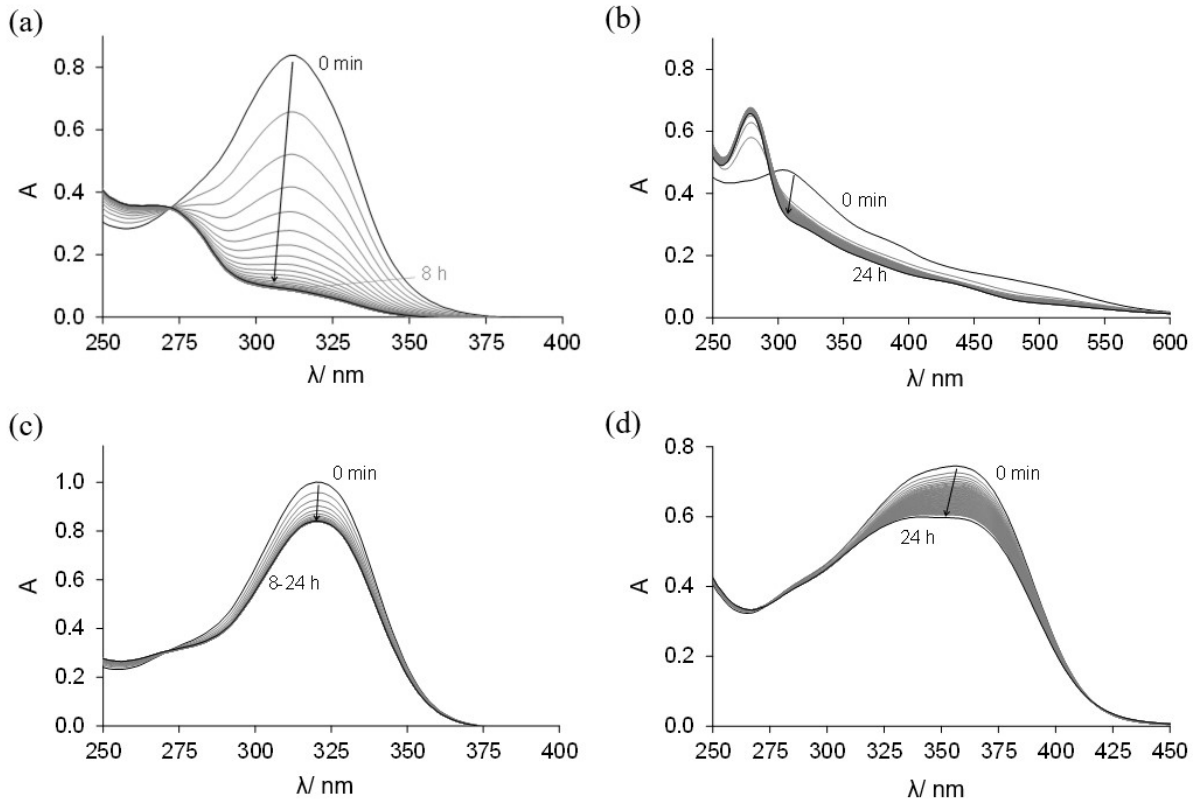

Figure S13. UV–vis absorption spectra recorded for **HL²** at (a) pH 2 and (b) pH 11.7, and for **HL³** at (c) pH 2 and (d) pH 11.7 over time; {c_{ligand} = 50 μM; ℓ = 1 cm; t = 25.0 °C}.

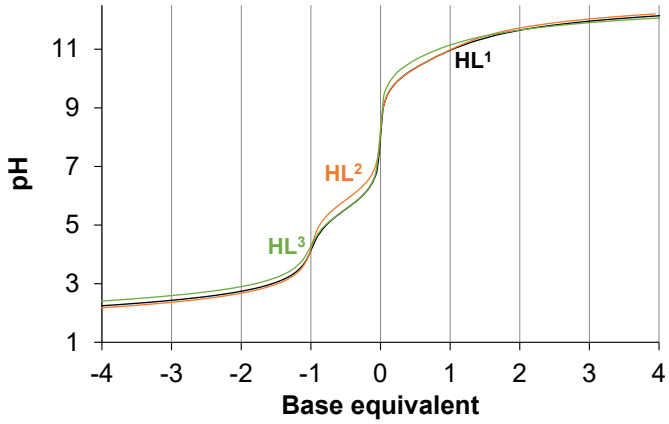

Figure S14. pH-potentiometric titration curves of the studied proligands **HL¹–HL³** in 30% (*v*/*v*) DMSO/H_2O. Base equivalent: ($n_{KOH} - n_{HCl}$) / n_{ligand}; {ℓ = 1 cm; I = 0.1 M (KCl); t = 25.0 °C}.

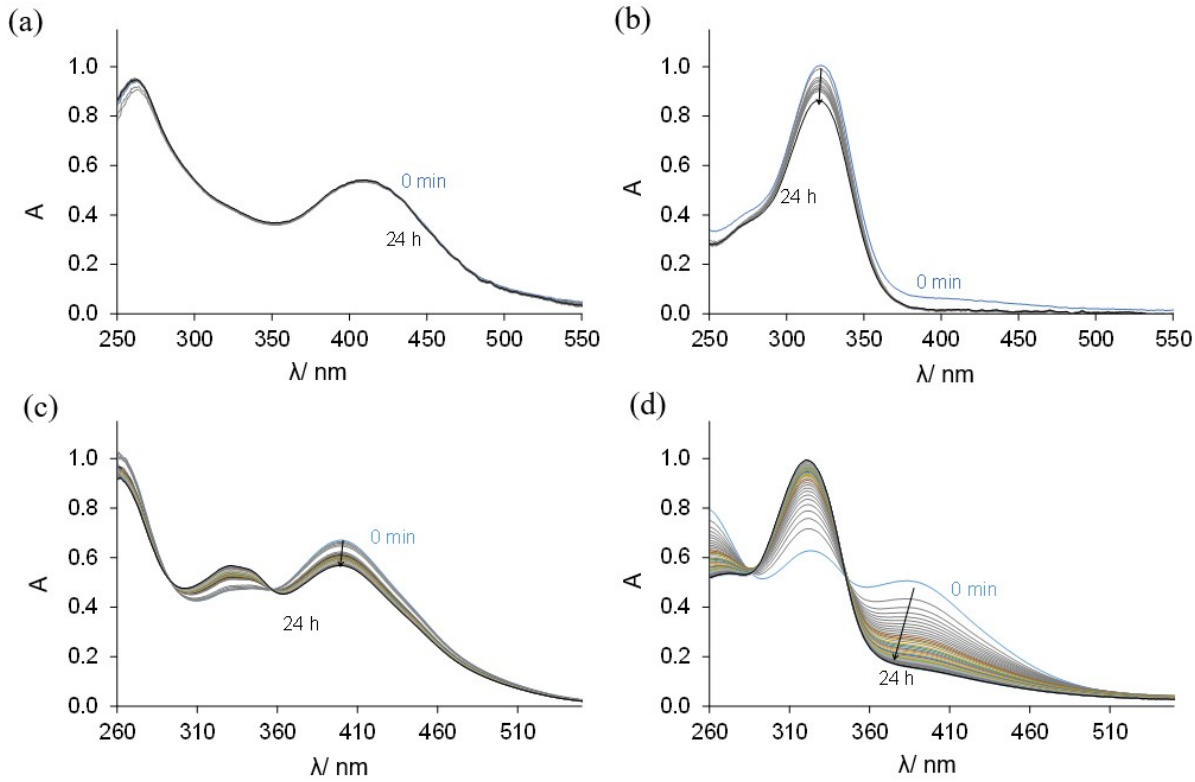

Figure S15. UV–vis absorption spectra recorded for (a) complex **2** at pH 2 and for complex **5** (b) at pH 2, (c) complex **2** in DMSO, and (d) complex **2** at pH 7.4 over time; {$c_{complex}$ = 21 μM (**2**) or 23 μM (**5**); ℓ = 1 cm; t = 25.0 °C}.

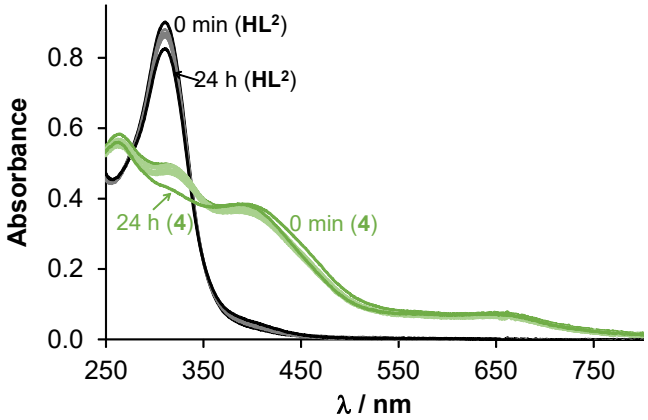

Figure S16. UV–vis absorption spectra recorded for complex **4** (green lines) and **HL²** (black lines) at pH 11.7 over time in the glove box; {c = 23 μM; ℓ = 1 cm; t = 25.0 °C}.

4. Spectroelectrochemistry

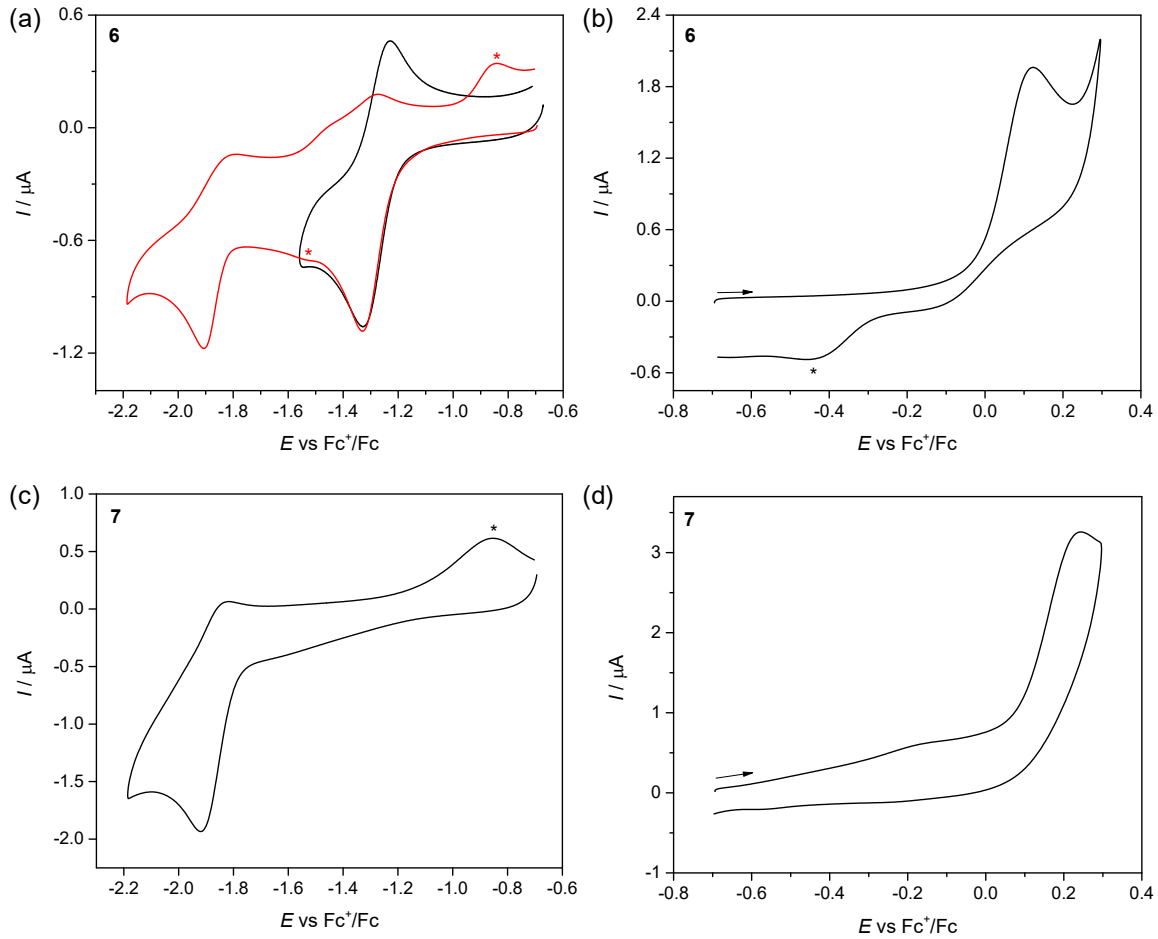

Figure S17. Cyclic voltammograms of the nickel complex **6** (a) in the cathodic and (b) in the anodic part, as well as of the zinc(II) complex **7** (c) in the cathodic and (d) in the anodic part in DMSO/nBu$_4$NPF$_6$ (Pt working electrode, scan rate: 100 mV s^{-1}). Asterisk indicates the follow up products formed upon reduction and oxidation, respectively.

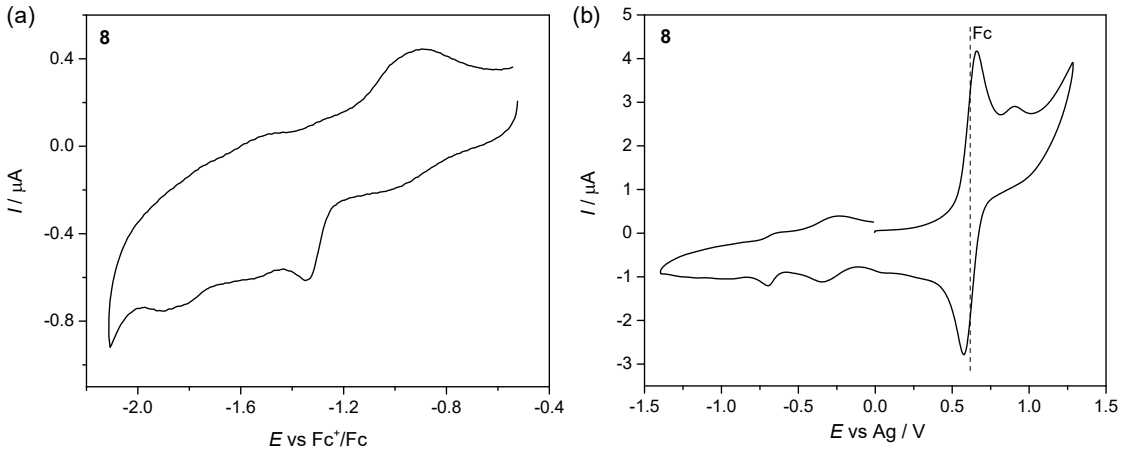

Figure S18. Cyclic voltammograms of palladium(II) complex **8** (a) in the cathodic part and (b) in both the anodic and cathodic parts in the presence of ferrocene in DMSO/nBu$_4$NPF$_6$ (Pt working electrode, scan rate: 100 mV s^{-1}).

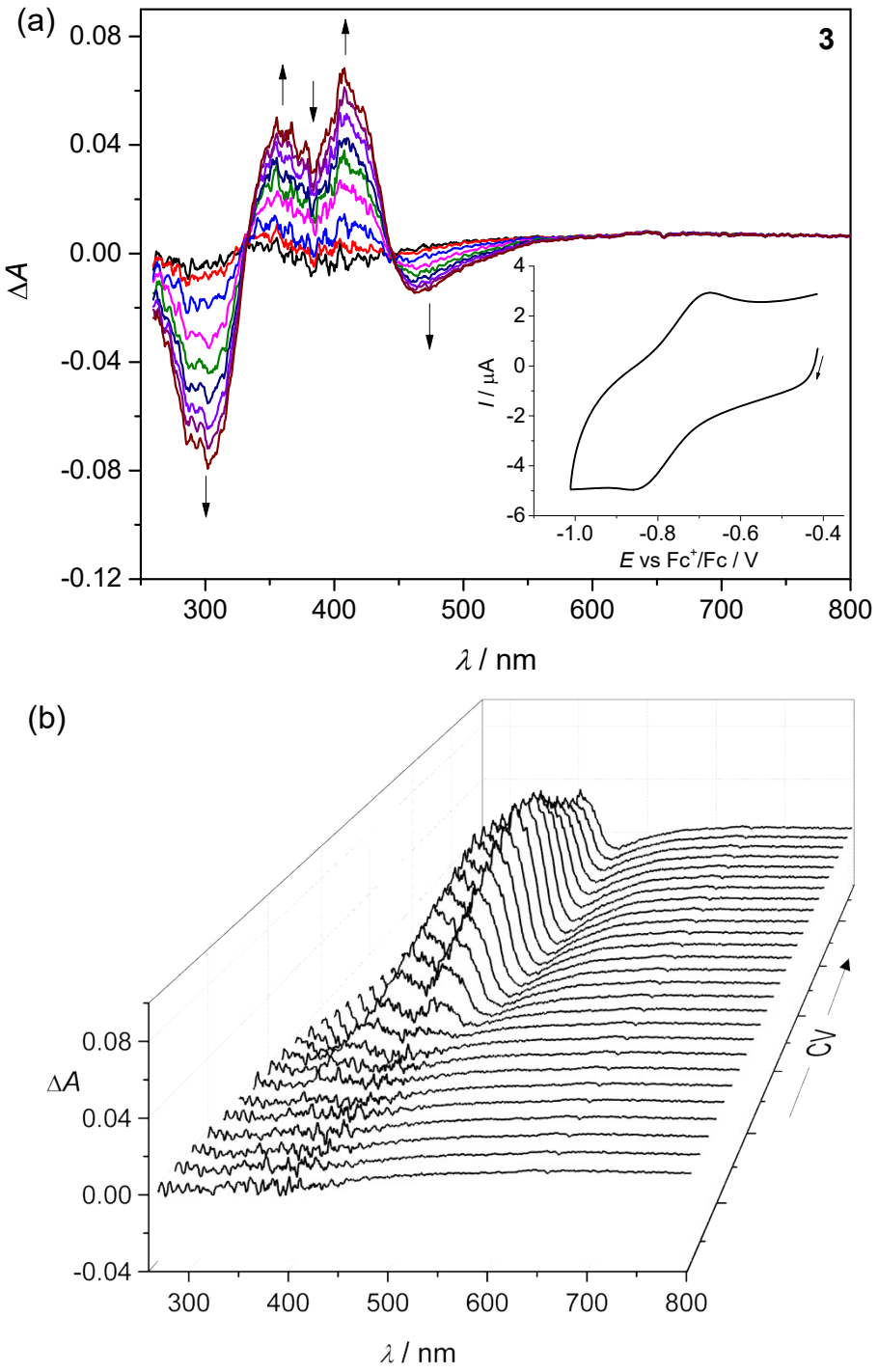

Figure S19. (a) Difference UV–vis–NIR spectra detected simultaneously during the *in situ* reduction of **3** in nBu$_4$NPF$_6$/DMSO in the region of the first cathodic peak (forward scan). Inset: respective cyclic voltammogram (Pt-microstructured honeycomb working electrode, scan rate v = 10 mV s^{-1}). (b) Difference UV–vis–NIR spectra taken during cyclic voltametric scan of **3** shown in 3D mode.

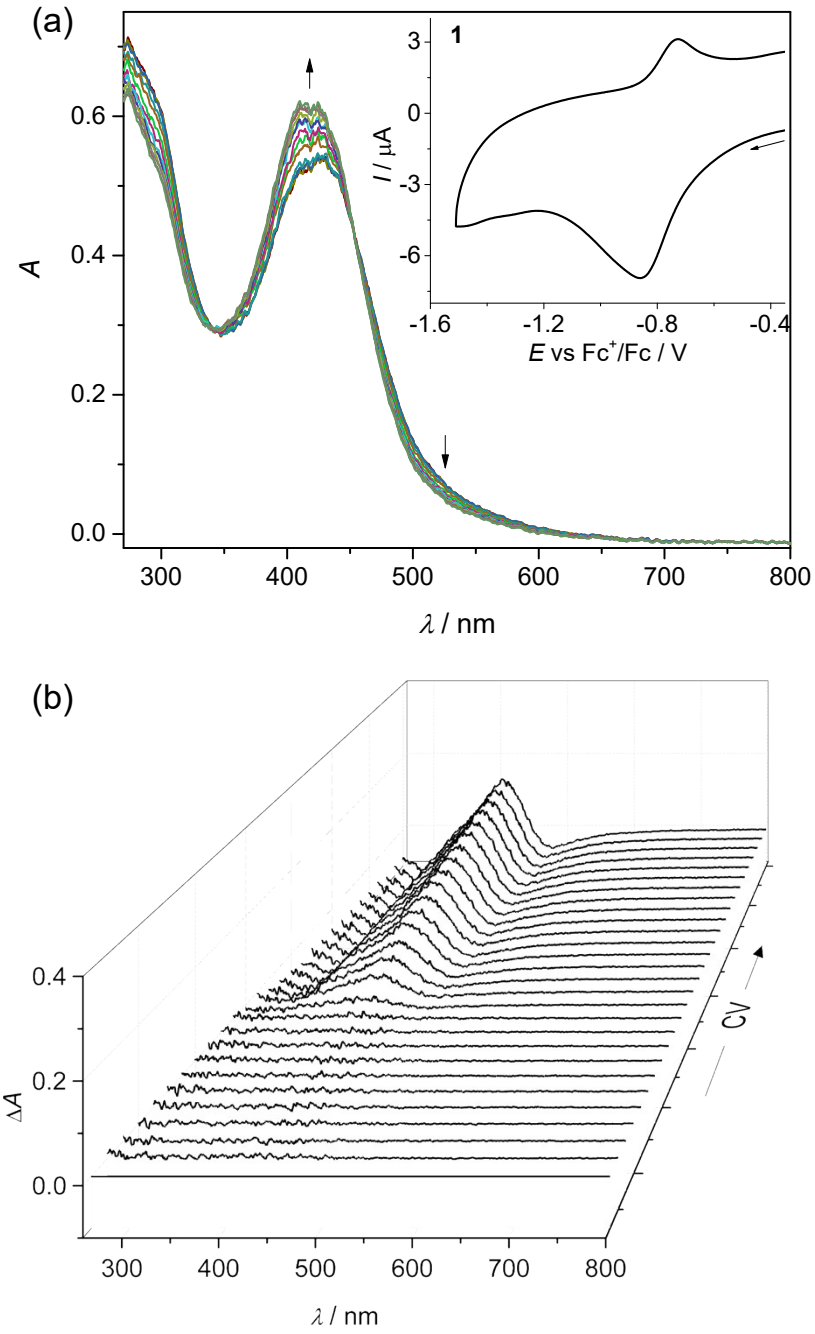

Figure S20. (a) UV–vis–NIR spectra detected simultaneously upon the *in situ* reduction of **1** in nBu$_4$NPF$_6$/DMSO in the region of the first cathodic peak; inset: respective cyclic voltammogram (Pt-microstructured honeycomb working electrode, scan rate v = 10 mV s^{-1}); (b) Difference UV–vis–NIR spectra taken upon cyclic voltametric scan of **1** shown in 3D mode.

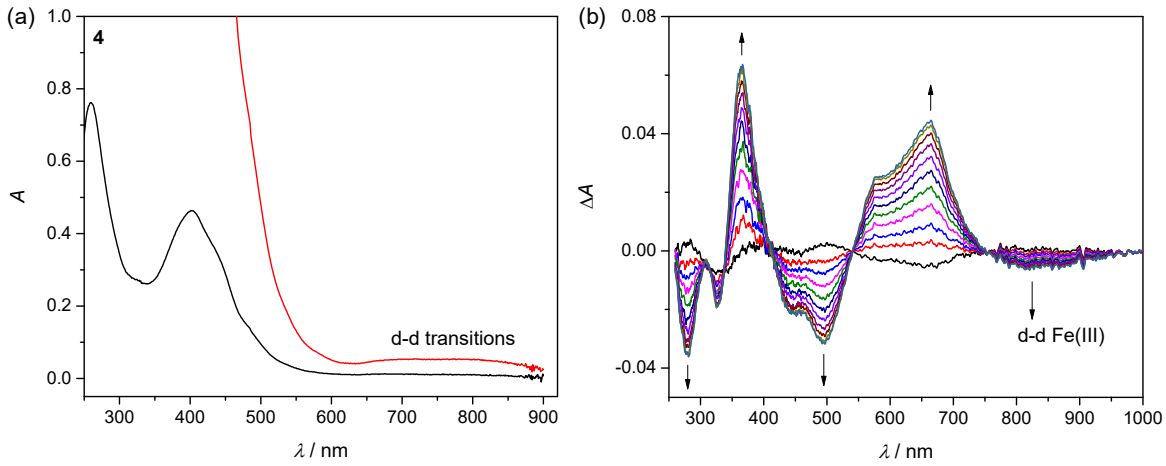

Figure S21. (a) UV–vis–NIR spectra of **4** in DMSO; (b) Spectroelectrochemistry of **4** in nBu$_4$NPF$_6$/DMSO in the region of the first cathodic peak - evolution of difference UV–vis–NIR spectra measured simultaneously upon forward scan (Pt-microstructured honeycomb working electrode, scan rate v = 10 mV s^{-1}).

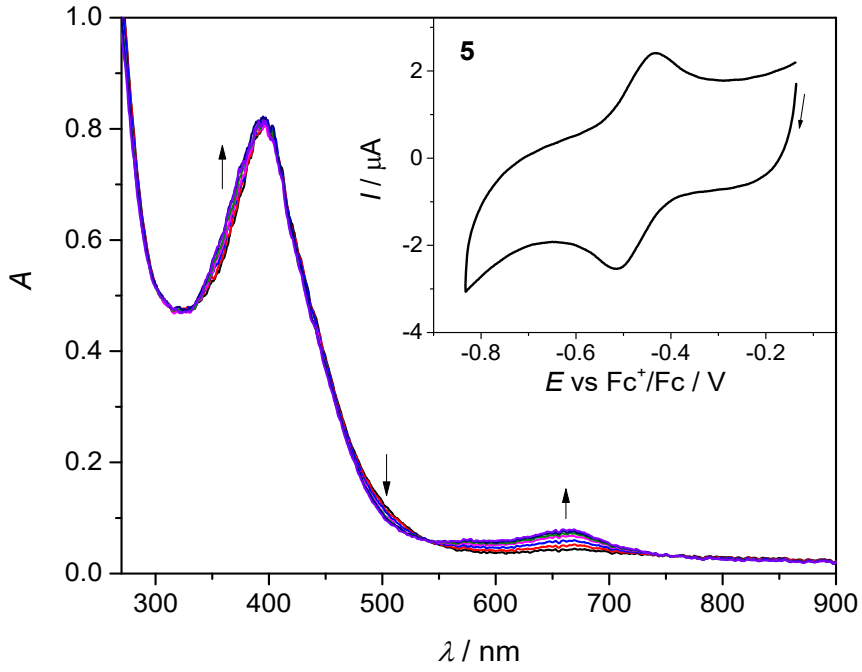

Figure S22. UV–vis–NIR spectra measured simultaneously upon the *in situ* reduction of **5** in nBu$_4$NPF$_6$/DMSO in the region of the first cathodic peak (forward scan); inset: respective cyclic voltammogram (Pt-microstructured honeycomb working electrode, scan rate v = 10 mV s^{-1}).

5. NCI-60 One-Dose Screen

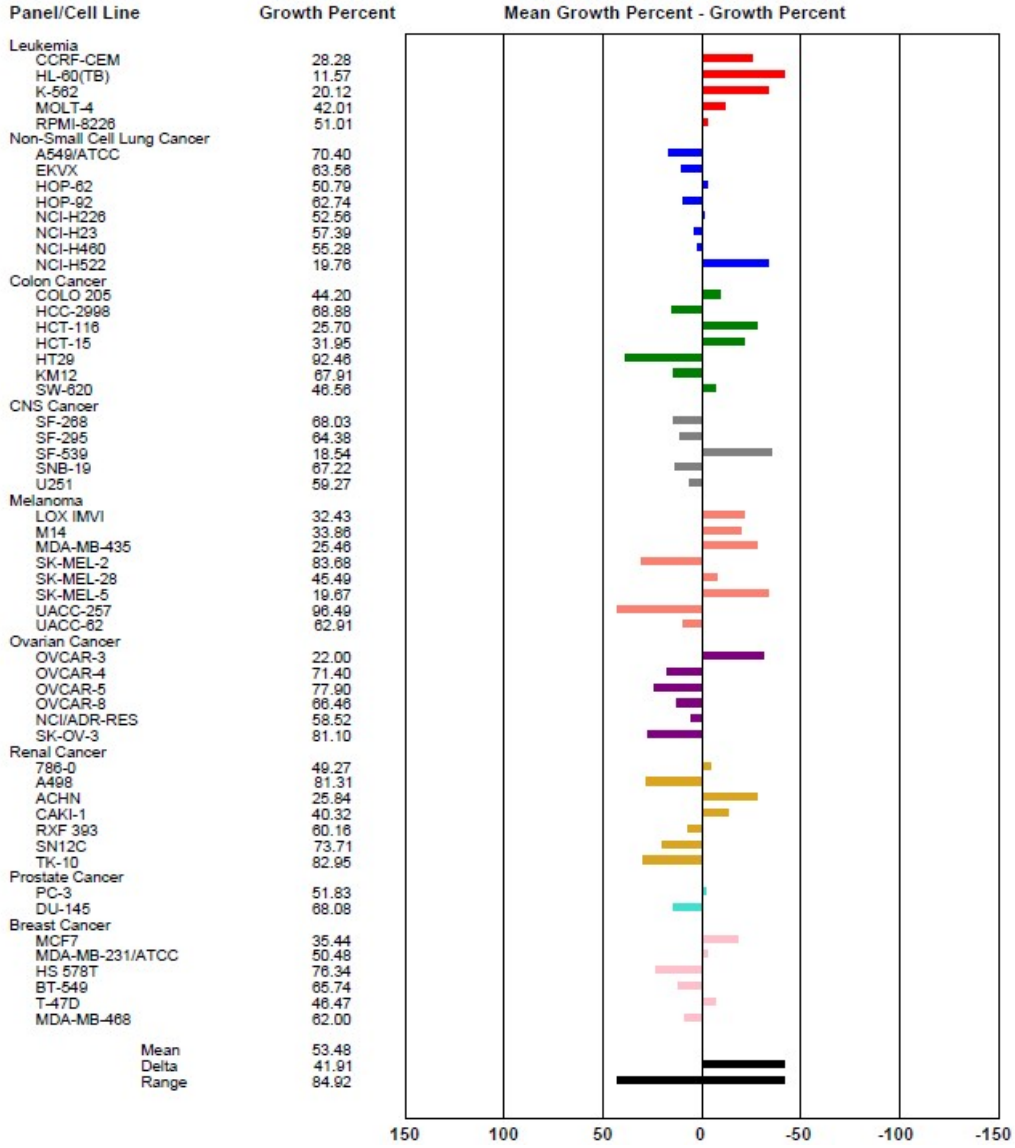

Figure S23. One dose mean graph for **HL**[1].

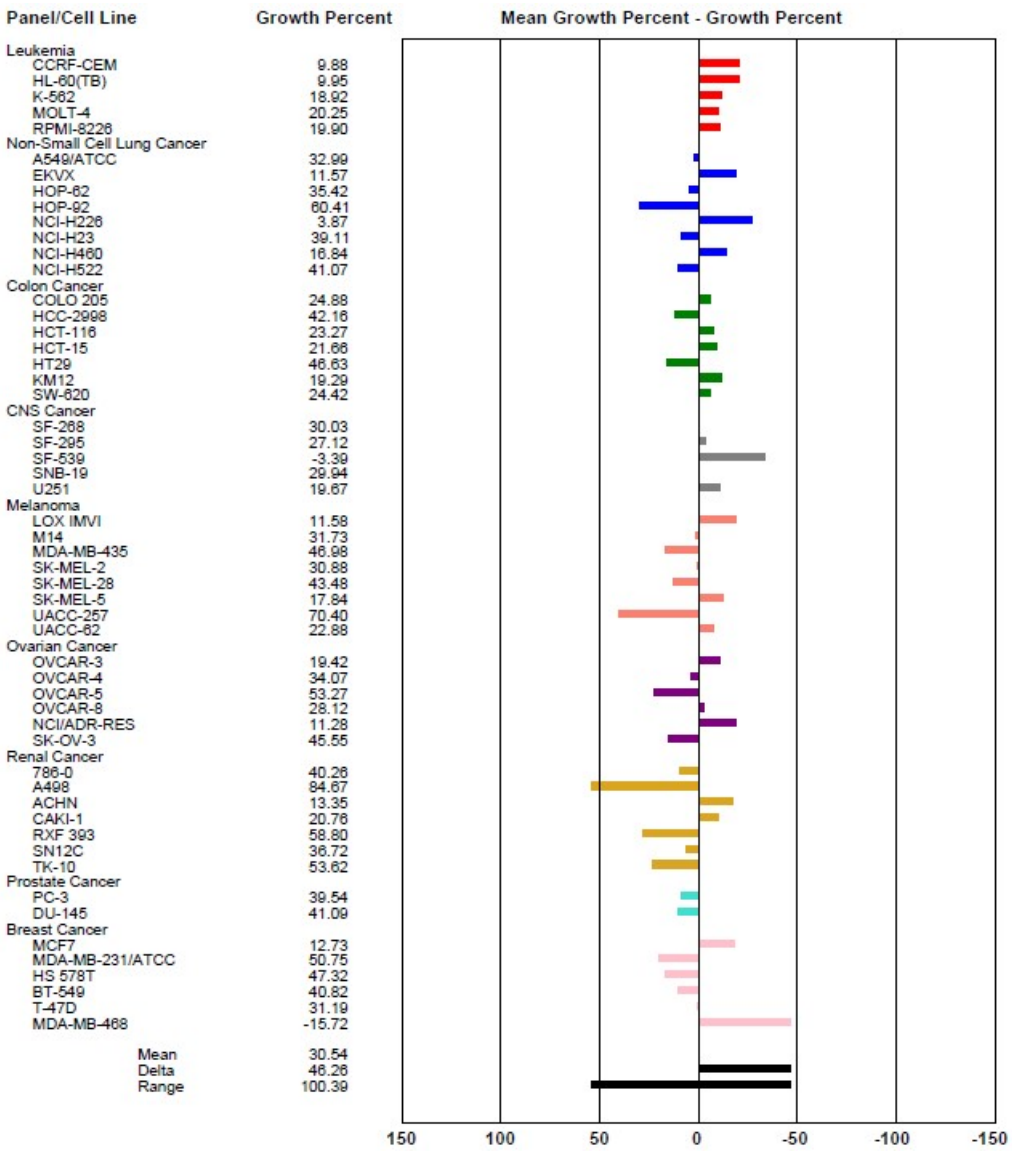

Figure S24. One dose mean graph for **HL²**.

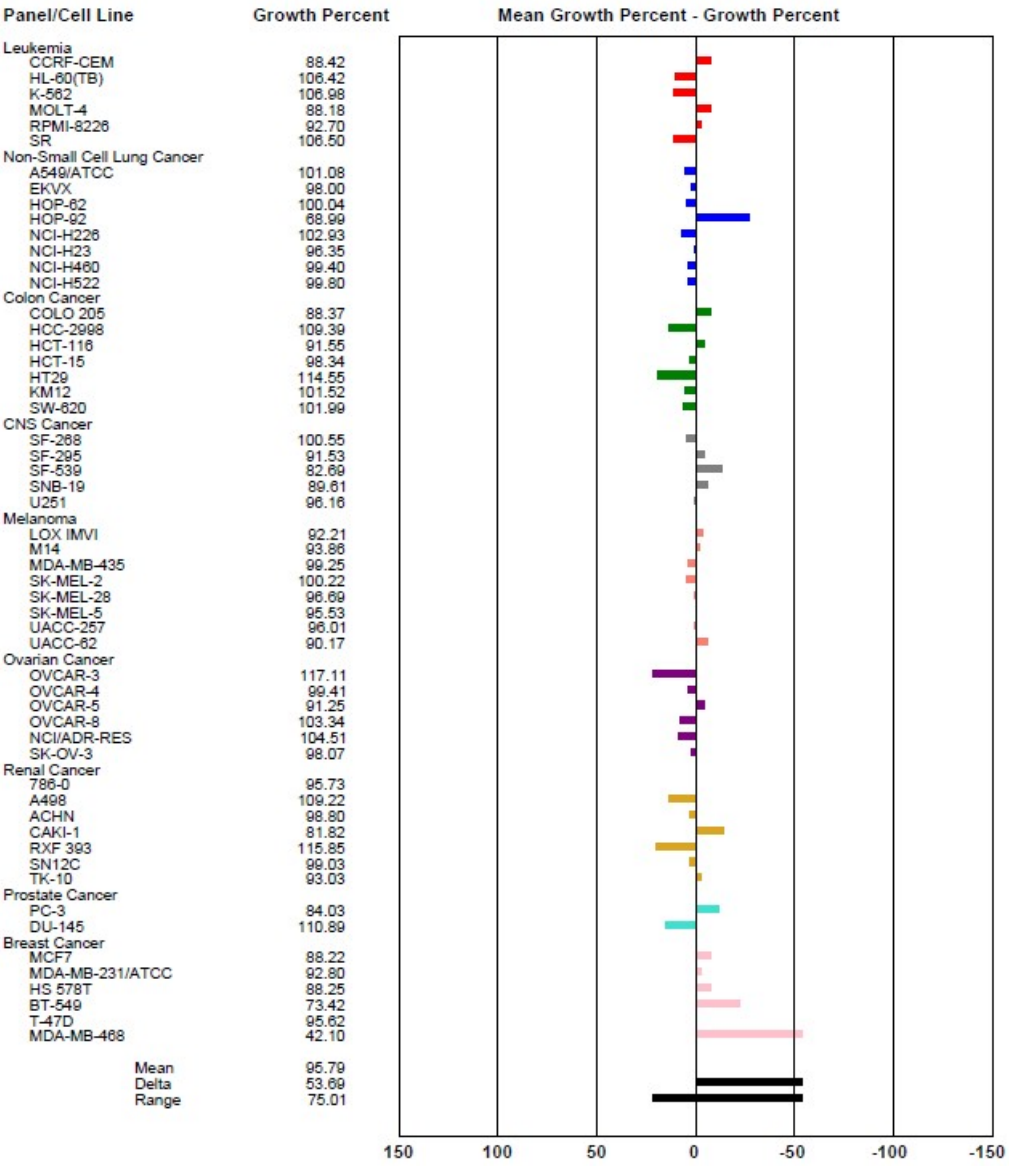

Figure S25. One dose mean graph for **3**.

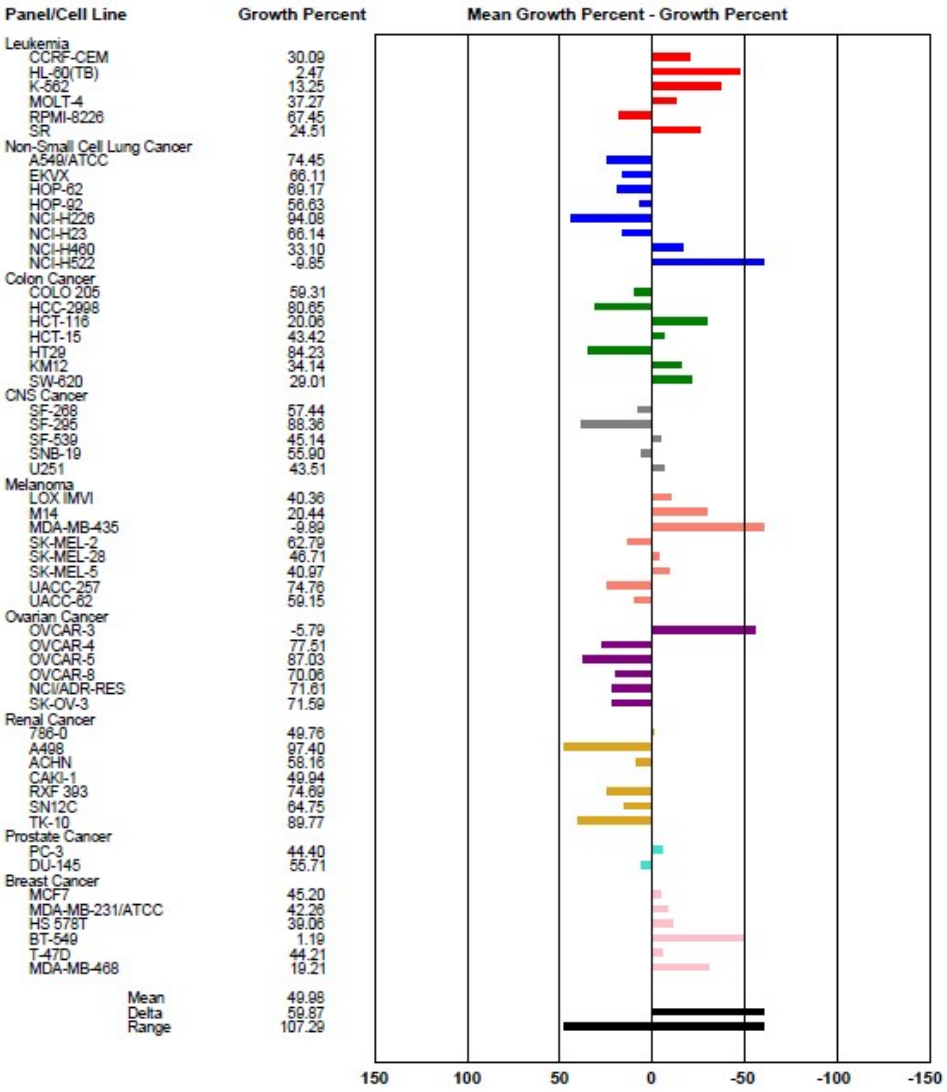

Figure S26. One dose mean graph for **6**.

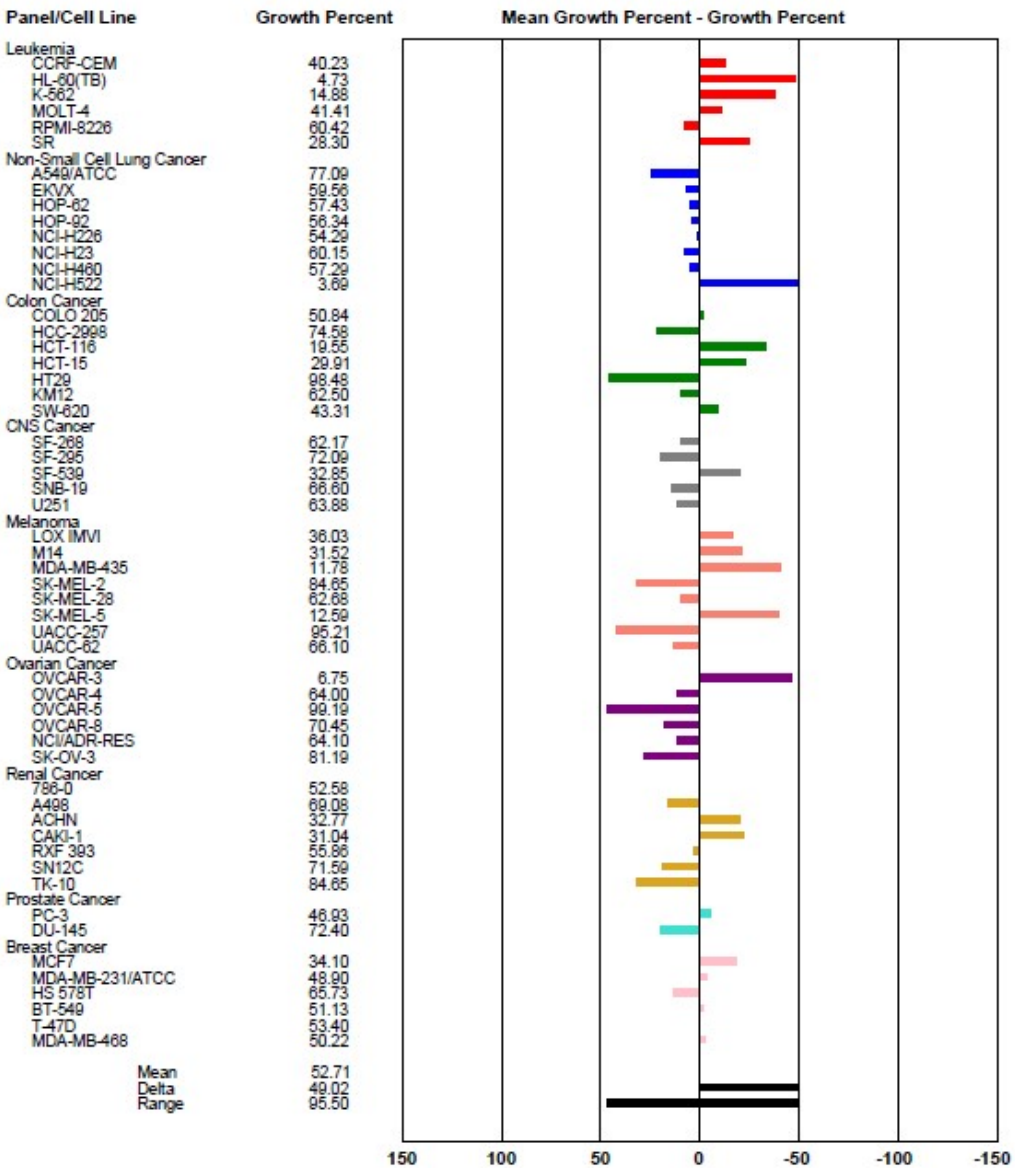

Figure S27. One dose mean graph for **7**.

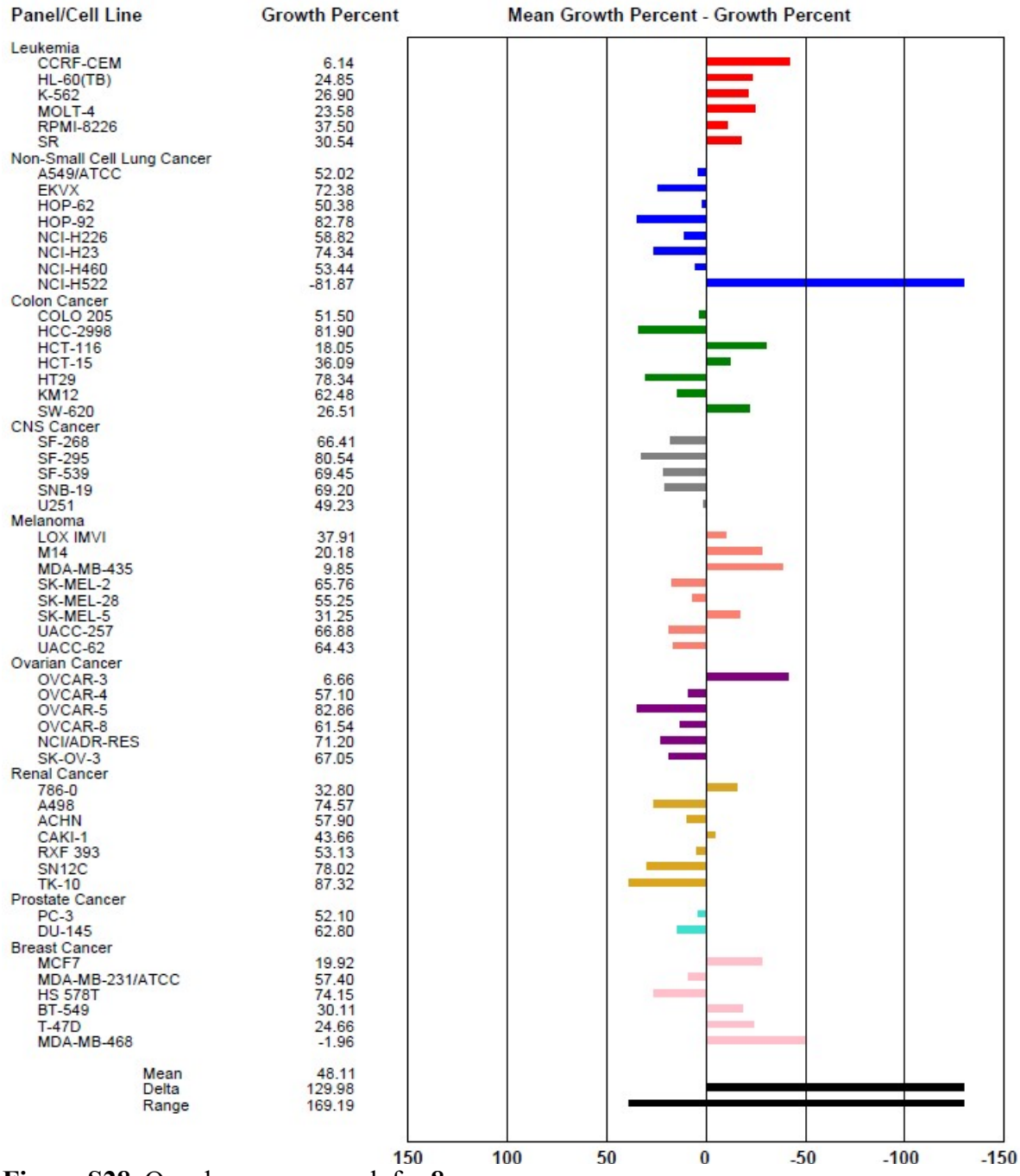

Figure S28. One dose mean graph for **8**.

6. NCI-60 5-Dose Screen

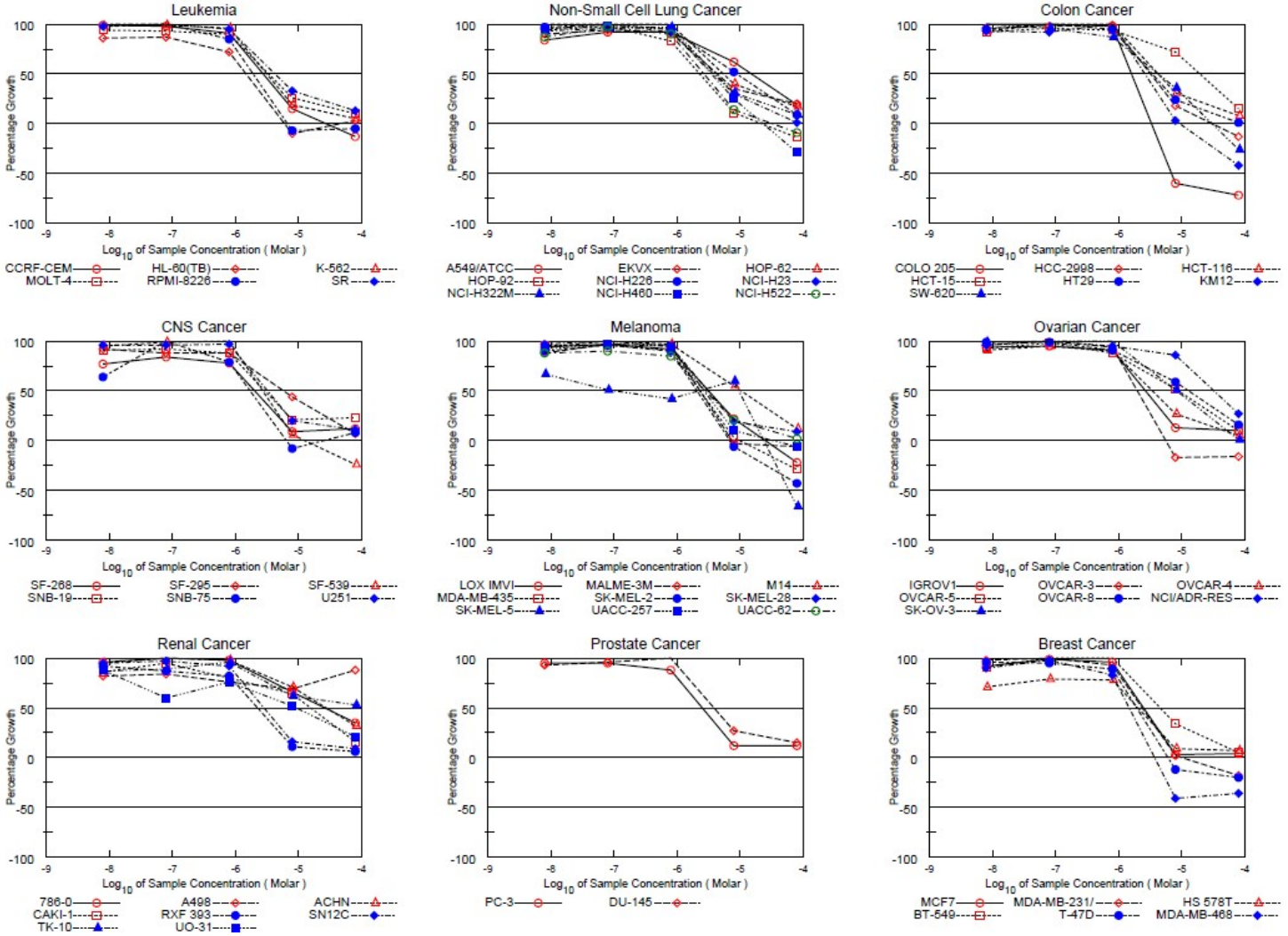

Figure S29. Dose response curves for **1**.

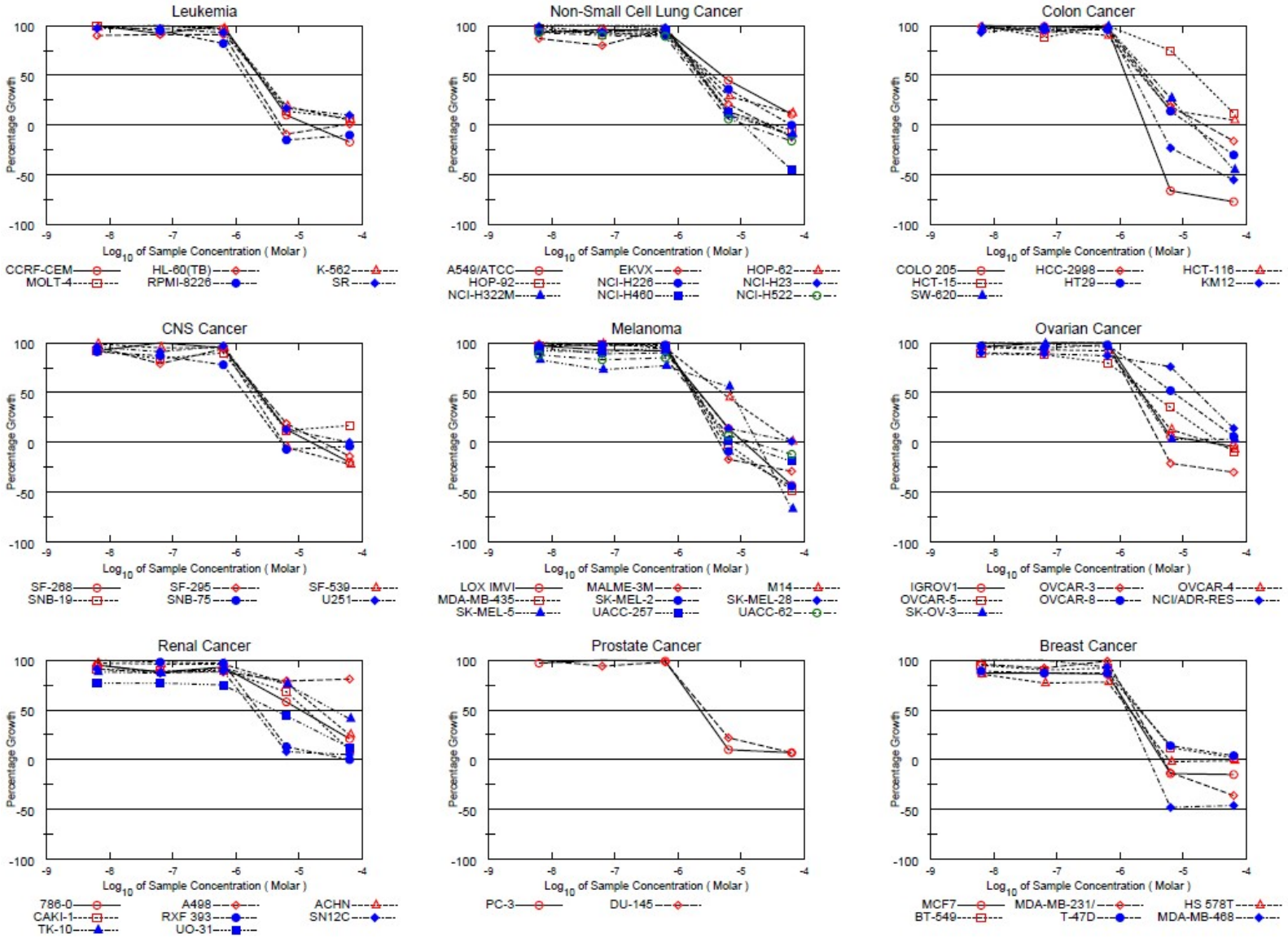

Figure S30. Dose response curves for **2**.

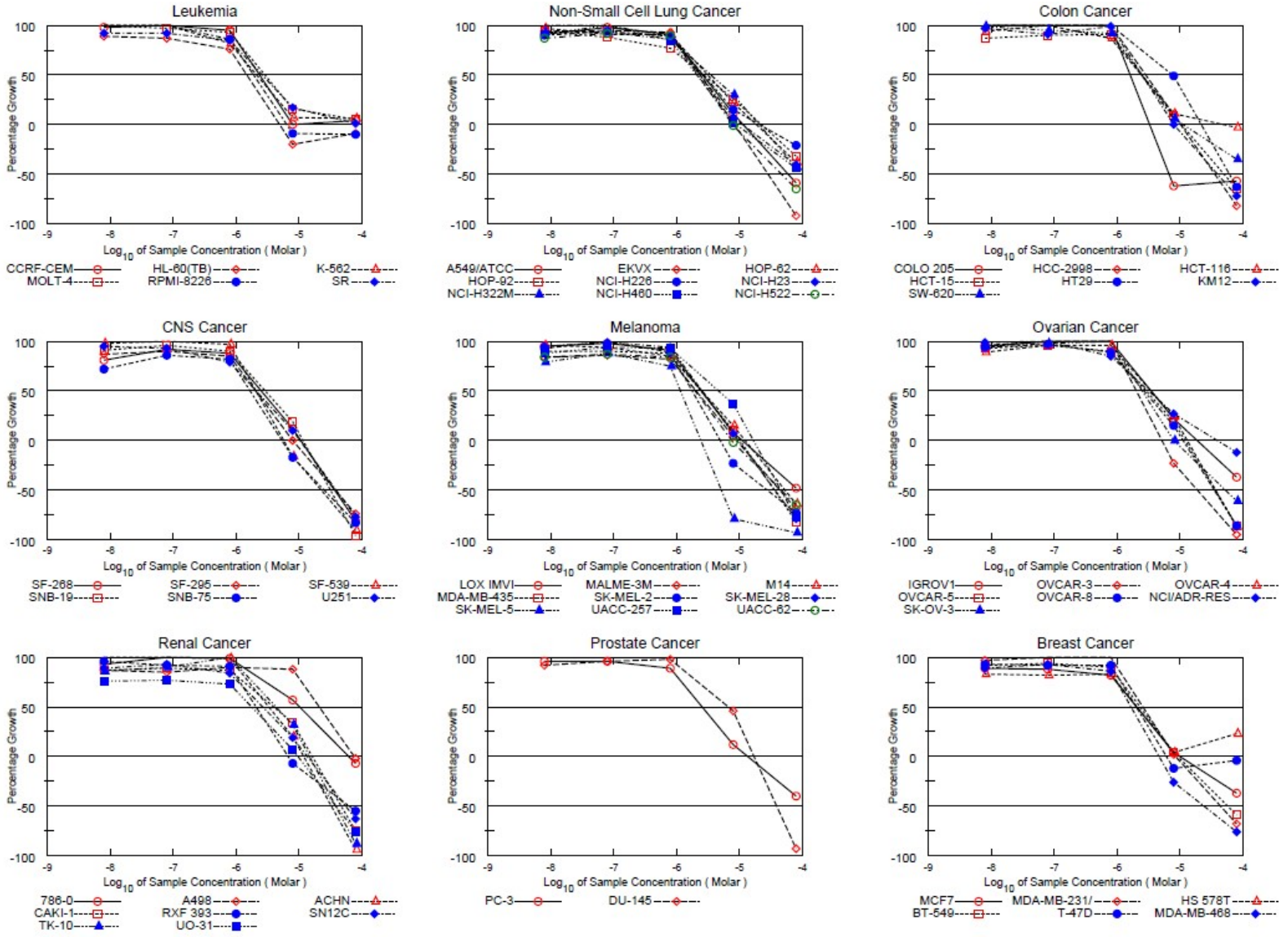

Figure S31. Dose response curves for **4**.

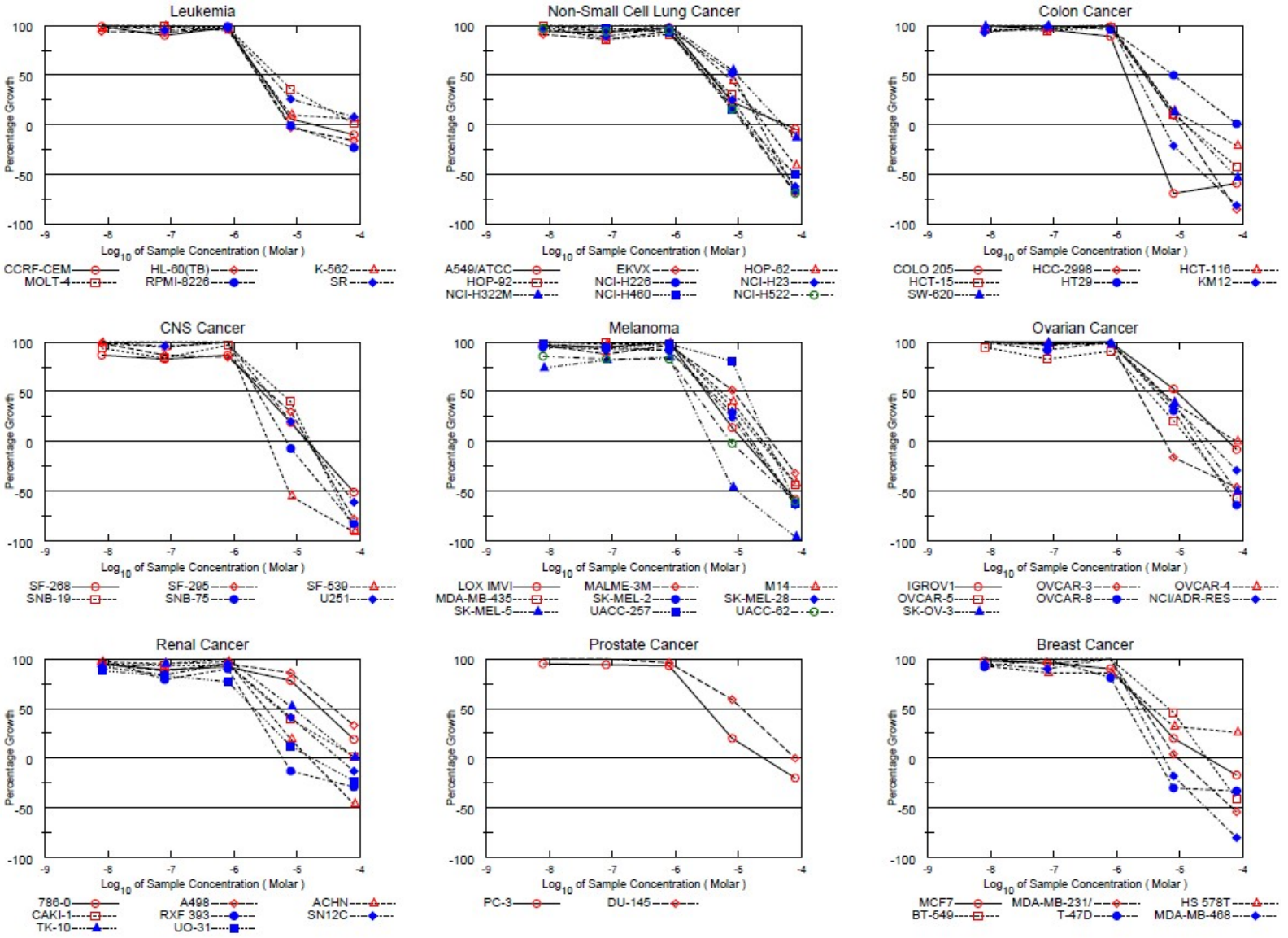

Figure S32. Dose response curves for **5**.

7. Molecular docking

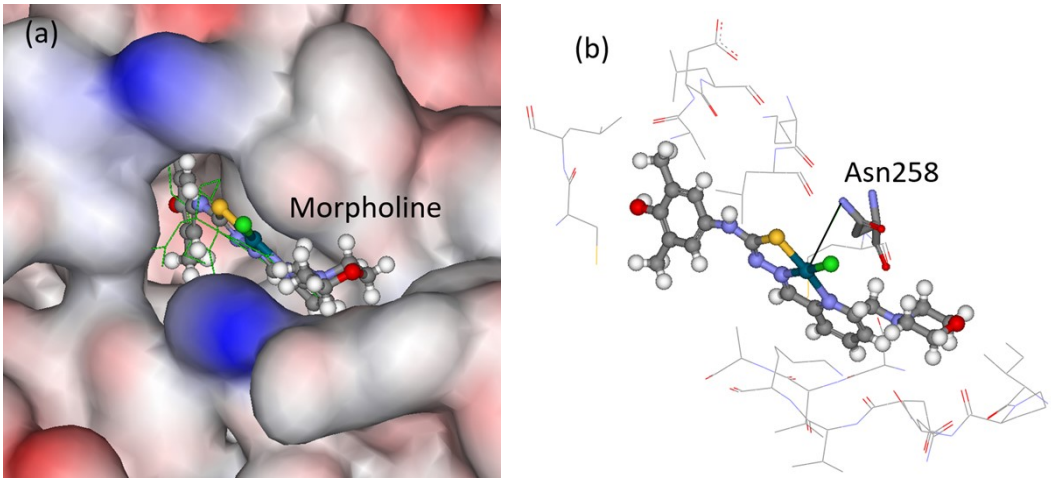

Figure S33. (a) The docked pose of **8** (ball-and-stick) in the colchicine site of tubulin. The co-crystalized ligand (LOC) is shown in line format (green), its hydrogen atoms are not shown for clarity. The protein surface is rendered with blue color depicting regions with a partial positive charge on the surface, red color depicting regions with a partial negative charge and grey showing neutral areas. (b) The predicted binding of complex **8**, amino acids within 5 Å are shown in line format. Complex formation of the amide side chain of βAsn258 with the Pd(II) could occur as shown in this docking image (black solid line, 3.7 Å).